NASA/TM–2018–220102

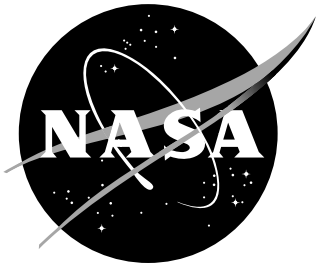

Output Measurement Equations for Flexible Aircraft Flight Dynamics

Jared A. Grauer
Langley Research Center, Hampton, Virginia

Matthew J. Boucher
Armstrong Flight Research Center, Edwards, California

October 2018

The NASA STI Program Office ... in Profile

Since its founding, NASA has been dedicated to the advancement of aeronautics and space science. The NASA Scientific and Technical Information (STI) Program Office plays a key part in helping NASA maintain this important role.

The NASA STI Program Office is operated by Langley Research Center, the lead center for NASA's scientific and technical information. The NASA STI Program Office provides access to the NASA STI Database, the largest collection of aeronautical and space science STI in the world. The Program Office is also NASA's institutional mechanism for disseminating the results of its research and development activities. These results are published by NASA in the NASA STI Report Series, which includes the following report types:

- TECHNICAL PUBLICATION. Reports of completed research or a major significant phase of research that present the results of NASA programs and include extensive data or theoretical analysis. Includes compilations of significant scientific and technical data and information deemed to be of continuing reference value. NASA counterpart of peer-reviewed formal professional papers, but having less stringent limitations on manuscript length and extent of graphic presentations.
- TECHNICAL MEMORANDUM. Scientific and technical findings that are preliminary or of specialized interest, e.g., quick release reports, working papers, and bibliographies that contain minimal annotation. Does not contain extensive analysis.
- CONTRACTOR REPORT. Scientific and technical findings by NASA-sponsored contractors and grantees.
- CONFERENCE PUBLICATION. Collected papers from scientific and technical conferences, symposia, seminars, or other meetings sponsored or co-sponsored by NASA.
- SPECIAL PUBLICATION. Scientific, technical, or historical information from NASA programs, projects, and missions, often concerned with subjects having substantial public interest.
- TECHNICAL TRANSLATION. English-language translations of foreign scientific and technical material pertinent to NASA's mission.

Specialized services that complement the STI Program Office's diverse offerings include creating custom thesauri, building customized databases, organizing and publishing research results ... even providing videos.

For more information about the NASA STI Program Office, see the following:

- Access the NASA STI Program Home Page at ***http://www.sti.nasa.gov***
- E-mail your question via the Internet to help@sti.nasa.gov
- Fax your question to the NASA STI Help Desk at (301) 621–0134
- Phone the NASA STI Help Desk at (301) 621–0390
- Write to:
  NASA STI Help Desk
  NASA Center for AeroSpace Information
  7115 Standard Drive
  Hanover, MD 21076–1320

NASA/TM–2018–220102

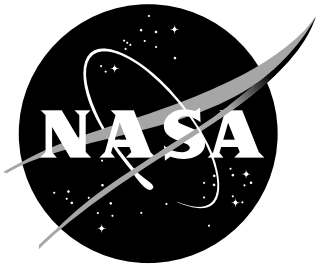

Output Measurement Equations for Flexible Aircraft Flight Dynamics

Jared A. Grauer
Langley Research Center, Hampton, Virginia

Matthew J. Boucher
Armstrong Flight Research Center, Edwards, California

National Aeronautics and
Space Administration

Langley Research Center
Hampton, Virginia 23681-2199

October 2018

Available from:

NASA STI Program / Mail Stop 148
NASA Langley Research Center
Hampton, VA 23681-2199
Fax: 757-864-6500

Abstract

A summary of output measurement equations for onboard sensors used in flight testing flexible aircraft is presented. These equations include the effects of structural flexibility and are considerably more complex than the standard equations for rigid-body aircraft. The output equations discussed include accelerations from linear and angular accelerometers, strains, angular rates, Euler angles, true airspeed, and air flow angles. The output equations are derived in full form and then simplified. Linearized output equations, suitable for state-space or transfer function models, are also developed. Example flight test data from the X-56A subscale aeroelastic demonstrator is discussed for reference.

Contents

Nomenclature

Roman

$\mathbf{a}$	acceleration vector, ft/s^2
$\boldsymbol{a}$	accelerometer output vector, g
a_x, a_y, a_z	accelerometer output components, g
B	aircraft body reference frame
$B^\star$	aircraft mass center, origin of reference frame B
$\mathbf{b}_1$, $\mathbf{b}_2$, $\mathbf{b}_3$	orthonormal basis vectors fixed in reference frame B
C	point at which a sensor is installed in the undeformed aircraft
C_D, C_L	stability-axis nondimensional aerodynamic force coefficients
C_{Q_k}	nondimensional generalized-force coefficient
C_X, C_Y, C_Z	body-axis nondimensional aerodynamic force coefficients
$\bar{c}$	wing mean aerodynamic chord, ft
D	location of a sensor on the aircraft undergoing structural deformation
$\mathbf{f}$	force vector, lbf
$\mathbf{f}_a$	aerodynamic force vector, lbf
$\mathbf{f}_g$	gravitational force vector, lbf
$\mathbf{f}_p$	propulsive force vector, lbf
g	acceleration due to gravity, ft/s^2
k	vibration mode index number
M	number of vibration modes
m	aircraft mass, slug
m_k	vibration mode generalized mass, slug
N	Newtonian reference frame
$\mathbf{n}_1$, $\mathbf{n}_2$, $\mathbf{n}_3$	orthonormal basis vectors fixed in reference frame N
O	origin of reference frame N
p, q, r	body-axis angular rate components, rad/s
$\bar{q}$	dynamic pressure, lbf/ft^2
$\mathbf{r}$	position vector, ft
S	wing reference area, ft^2
t	time, s
u, v, w	body-axis velocity components, ft/s
V	true airspeed, ft/s
$\mathbf{v}$	velocity vector, ft/s
X_p, Y_p, Z_p	body-axis propulsion forces, lbf
$\times$	cross product
x, y, z	position components of mass center $B^\star$, ft
x_s, y_s, z_s	position components of installed sensor location C, ft

Greek

$\boldsymbol{\alpha}$	angular acceleration vector, rad/s^2
α	angle of attack, rad
β	sideslip angle, rad
Δ	perturbation value
δ_e	elevator deflection, rad
ϵ	strain
ζ_k	vibration mode damping ratio
η	vibration mode generalized displacement
μ	flank angle, rad
ν_{k_ϕ}, ν_{k_θ}, ν_{k_ψ}	components of angular vibration mode shape at the sensor, rad
ϕ, θ, ψ	roll, pitch, and yaw Euler angles, rad
ϕ_{k_x}, ϕ_{k_y}, ϕ_{k_z}	components of vibration mode shape at the sensor, ft

ψ_k	vibration strain mode shape at the sensor
$\boldsymbol{\omega}$	angular velocity vector, rad/s
ω_k	vibration mode natural frequency, rad/s

Subscripts

0	reference value
D	sensor location

Superscripts

$\dot{}$	time derivative

Acronyms

EGI	embedded GPS and INS
FEM	finite element model
GPS	global positioning system
GVT	ground vibration test
INS	inertial navigation system
ITAR	International Traffic in Arms Regulations
SW1B	first symmetric wing bending
SW1T	first symmetric wing torsion

1 Introduction

Models describing the outputs of sensors aboard idealized rigid aircraft are well known and routinely used in flight dynamics analyses such as simulation, control design, and system identification [1–4]. For actual aircraft, measured data contain additional contributions from the vibration of the aircraft structure which is not captured by the conventional models. In some cases, filters can be applied to remove unwanted structural contributions from the data [5]. However, this may not be appropriate if the structural flexibility significantly impacts the aircraft motion or if the vibration is of interest, as in aeroelastic analysis.

Although many sources present output measurement models for sensors considering structural deformations, for example references [6–9], a limited subset of relevant sensors are typically discussed and/or only linearized equations are provided. For new and unique problems that arise in research, however, the more complete output equations containing the nonlinearities inherent in the measurements are first needed before any simplifying assumptions can be carefully considered and applied. To the authors' knowledge, such a presentation is not available in the current literature.

The purpose of this report is (1) to develop and compile nonlinear output measurement models of common sensors on flexible aircraft for flight dynamics work; (2) to apply approximations to simplify those output measurement equations for various conditions; and (3) to discuss the effects of structural flexibility on the measurements. Section 2 presents example flight test data for the X-56A aeroelastic demonstrator where contributions from the structural deformations were significant compared to the rigid-body contributions. In section 3, Kane's method is used to develop kinematic relationships for the sensed quantities. The structural deformations are then expanded as a linear combination of orthogonal vibration modes. From these definitions, output equations for linear and rotational accelerometers, strain gauges, rate gyros, Euler angles, airspeed, and air flow angles are developed in section 4. Where appropriate, useful approximations are identified and simplified models are developed. Linearized models, suitable for state-space or transfer function, are also derived. Concluding remarks are then given in section 5.

2 Motivational Example

The X-56A Multi-Use Technology Testbed (MUTT) is a subscale aeroelastic demonstrator designed for studying aeroelastic modeling and active flutter suppression technologies [10, 11]. Figure 1 shows a photograph of the X-56A in flight, and figure 2 shows a three-view schematic of the aircraft. The X-56A has a lambda-wing planform with winglets. Two engines are mounted above the aft section of the center body. The landing gear are fixed and arranged in a tricycle configuration. There are 10 control surfaces: four along the trailing edges of each wing and two along the trailing edges of the center body.

Measured flight test data for a subset of sensors over a portion of one maneuver are shown in figure 3. Frequency transforms of this data are shown in figure 4 as amplitude spectra. Due to ITAR restrictions, numerical values have been removed from these plots. The elevator deflection was defined as the average symmetric deflection of the middle two wing flaps which were measured using potentiometers. Airspeed was computed using data from a pitot tube mounted on an airdata boom protruding from the aircraft nose and other measurements of the ambient atmosphere. The airdata boom also contained air flow angle vanes which provided the angle of attack measurement. Pitch angle was measured using an embedded GPS/INS (EGI) system located near the nominal aircraft center of mass. Pitch rate was measured using rate gyroscopes near the aircraft nose, and these measurements were smoothly differentiated to provide pitch acceleration measurements. The vertical accelerometer data shown was from a sensor installed in the left wing near the leading edge. The strain data was from a bending strain gauge installed near the wing root of the right wing.

The elevator command for this maneuver included a multisine input [3] with 61 discrete frequencies to excite the short period, first symmetric wing bending (SW1B) mode, and first symmetric wing torsion (SW1T) mode while keeping the aircraft near the straight and level reference condition. The general bandwidths for these resonances are annotated in figure 4. Higher-frequency structural modes were also present in the data due to the excitation onset, ambient turbulence, and dynamic coupling of the structure. Mode shapes for

the SW1B and SW1T modes, depicted in figure 5, were computed using a finite element model (FEM) tuned to ground vibration test (GVT) data. The mode numbers 7 and 9 used to indicate the SW1B and SW1T modes correspond to the numbering used in the FEM.

As seen most clearly by the frequency transforms in figure 4, several measurements had content near the structural responses that were equal to or greater in amplitude than the responses from the rigid-body short-period mode. This characteristic is due to the structural flexibility designed into the X-56A aircraft, and accurate modeling requires measurement models that consider the flexibility of the vehicle structure. Throughout this report, this flight test data will be referenced to discuss specific sensor measurements.

3 Kinematic Relationships

This section defines the position, velocity, and acceleration of an arbitrary point on the aircraft needed to develop the sensor output measurement equations in the next section. These kinematic terms are first presented in a compact vector form. Next, the structural deformations of the aircraft are modeled using a finite set of the orthogonal vibration modes as basis functions. Lastly, the kinematic quantities are written in scalar forms using the developed structural deformations and conventional aircraft flight dynamics nomenclature.

Vector Definitions

A schematic for a generic flexible aircraft is shown in figure 6. The Newtonian (inertial) reference frame is denoted N. The orthonormal vectors $\mathbf{n}_1$, $\mathbf{n}_2$, and $\mathbf{n}_3$ are fixed in N and originate at point O. The notation used for this figure and in this section follows from reference [12], which is widely regarded for its simple and efficient representation. For example, kinematic quantities are developed without specialization to a particular reference frame, which increases the generality of the expressions and reduces complexity of the notation.

The aircraft body is denoted B and has its instantaneous mass center at point $B^\star$ with position $\mathbf{r}^{OB^\star}$. The mass center is not fixed to a physical point in the aircraft, but instead moves according to the distribution of mass, for example due to fuel burn. Three orthonormal vectors, $\mathbf{b}_1$, $\mathbf{b}_2$, and $\mathbf{b}_3$, originate at $B^\star$ and denote the aircraft body mean axes, which are formally defined such that the translational and angular momenta from unforced elastic deformation are zero [6]. Less rigorously, the mean axes can be thought of as the body axes of the aircraft in its undeformed jig shape, about which the structure vibrates. For truly rigid aircraft, the mean axes are identical to the body axes, where $\mathbf{b}_1$ points out the nose (x direction), $\mathbf{b}_2$ points out the right wing (y direction), and $\mathbf{b}_3$ points out the bottom of the aircraft (z direction). Frame B also has angular velocity $\boldsymbol{\omega}$ in N and angular acceleration $\boldsymbol{\alpha}$ in N. The mass center $B^\star$ has velocity ${}^N\mathbf{v}^{B^\star}$ in N and acceleration ${}^N\mathbf{a}^{B^\star}$ in N.

A given sensor is initially located at point C, which is fixed in B at $\mathbf{r}^{B^\star C}$. When the aircraft experiences structural deformation, the sensor location moves from C to point D along $\mathbf{r}^{CD}$ in B. The inertial position of the sensor when the aircraft has deformed is the sum of the position vectors

$$\mathbf{r}^{OD} = \mathbf{r}^{OB^\star} + \mathbf{r}^{B^\star C} + \mathbf{r}^{CD} \tag{1}$$

The inertial velocity at the sensor results from differentiating equation (1) in N with respect to time, as

$$
\begin{aligned}
{}^N\mathbf{v}^D &= \frac{{}^N d}{dt}(\mathbf{r}^{OD}) \\
&= \frac{{}^N d}{dt}(\mathbf{r}^{OB^\star}) + \frac{{}^N d}{dt}(\mathbf{r}^{B^\star C} + \mathbf{r}^{CD}) \\
&= \frac{{}^N d}{dt}(\mathbf{r}^{OB^\star}) + \boldsymbol{\omega}\times(\mathbf{r}^{B^\star C} + \mathbf{r}^{CD}) + \frac{{}^B d}{dt}(\mathbf{r}^{B^\star C} + \mathbf{r}^{CD}) \\
&= {}^N\mathbf{v}^{B^\star} + \boldsymbol{\omega}\times(\mathbf{r}^{B^\star C} + \mathbf{r}^{CD}) + {}^B\mathbf{v}^D
\end{aligned} \tag{2}
$$

where the superscript preceding the derivative symbol indicates the frame in which the derivative is taken. In developing equation (2), the theorem for differentiation in moving reference frames [12] was used, e.g.,

$$
\frac{{}^N d}{dt}(\mathbf{r}^{B^\star C}) = \frac{{}^B d}{dt}(\mathbf{r}^{B^\star C}) + \boldsymbol{\omega}\times\mathbf{r}^{B^\star C} \tag{3}
$$

The identity

$$
\frac{{}^B d}{dt}(\mathbf{r}^{B^\star C}) = \mathbf{0} \tag{4}
$$

was also used, which results from the initial sensor location being fixed in the body frame. The first term on the right side of equation (2) is the velocity of the aircraft mass center, the second term is the tangential velocity due to rotation of the aircraft and offset of the sensor location from the mass center, and the third term is the local velocity of the sensor due to structural deformation.

The acceleration at the sensor is obtained by differentiating equation (2) in N with respect to time,

$$
\begin{aligned}
{}^N\mathbf{a}^D &= \frac{{}^N d}{dt}({}^N\mathbf{v}^D) \\
&= \frac{{}^N d}{dt}({}^N\mathbf{v}^{B^\star}) + \frac{{}^N d}{dt}(\boldsymbol{\omega}\times(\mathbf{r}^{B^\star C} + \mathbf{r}^{CD})) + \frac{{}^N d}{dt}({}^B\mathbf{v}^D) \\
&= {}^N\mathbf{a}^{B^\star} + 2\boldsymbol{\omega}\times{}^B\mathbf{v}^D + \boldsymbol{\alpha}\times(\mathbf{r}^{B^\star C} + \mathbf{r}^{CD}) + \boldsymbol{\omega}\times[\boldsymbol{\omega}\times(\mathbf{r}^{B^\star C} + \mathbf{r}^{CD})] + {}^B\mathbf{a}^D
\end{aligned} \tag{5}
$$

Similar identities as in the development of equation (2) were applied, as well as the identity

$$
\boldsymbol{\alpha} = \frac{{}^B d\boldsymbol{\omega}}{dt} = \frac{{}^N d\boldsymbol{\omega}}{dt} \tag{6}
$$

which results from equation (3) because $\boldsymbol{\omega}\times\boldsymbol{\omega} = \mathbf{0}$. The first term on the right side of equation (5) is the acceleration of the aircraft mass center. The following three terms are the Coriolis, tangential, and centripetal accelerations, respectively. The last term is the local acceleration due to the structural deformation.

Equations (1), (2), and (5) constitute the inertial position, velocity, and acceleration of a sensor located at an arbitrary point D on a flexible aircraft undergoing structural deformation. The assumed deformations, so far in this discussion, can be arbitrarily large. Next, the structural deformations describing the motion of D relative to C will be parameterized using normal modes as basis functions, which restricts the analysis to small, elastic deformations.

Structural Deformation Model

When undergoing small elastic deformations in a vacuum, the vibrational modes of a structure each can be modeled as the second-order dynamic system

$$\ddot{\eta}_i + 2\zeta_i\omega_i\dot{\eta}_i + \omega_i^2\Delta\eta_i = \frac{\bar{q}S\bar{c}}{m_i}C_{Q_i} \tag{7}$$

about the reference condition. The modal state η_i represents the generalized displacement of the i^{th} vibration mode of the aircraft structure. The parameters m_i, ω_i, and ζ_i are the generalized mass, frequency, and damping ratio of the vibration mode. The term C_{Q_i} is the nondimensional generalized-force coefficient. Although in theory an infinite number of vibration modes exist, the modes considered are truncated to a finite set according to the intention for modeling the system and/or information content in available data. Unless otherwise indicated, the word "modal" in this report pertains to the vibration modes and not to generalized modal displacements of the short period mode, for example.

The deformation of aircraft structure, displacing the sensor from C to D, is expanded using the mode shapes of the M retained vibration modes as [6]

$$\mathbf{r}^{CD} = \sum_{k=1}^{M}\left(\phi_{k_x}\eta_k\mathbf{b}_1 + \phi_{k_y}\eta_k\mathbf{b}_2 + \phi_{k_z}\eta_k\mathbf{b}_3\right) \tag{8}$$

The terms ϕ_{k_x}, ϕ_{k_y}, and ϕ_{k_z} are the displacement components of the k^{th} mode shape along the body mean axes due to a unit displacement of η_k, as shown in figure 5 for example. The corresponding local velocities and accelerations due to the structural deformation are

$${}^B\mathbf{v}^D = \frac{{}^Bd}{dt}(\mathbf{r}^{CD}) = \sum_{k=1}^{M}\left(\phi_{k_x}\dot{\eta}_k\mathbf{b}_1 + \phi_{k_y}\dot{\eta}_k\mathbf{b}_2 + \phi_{k_z}\dot{\eta}_k\mathbf{b}_3\right) \tag{9}$$

$${}^B\mathbf{a}^D = \frac{{}^Bd}{dt}({}^B\mathbf{v}^D) = \sum_{k=1}^{M}\left(\phi_{k_x}\ddot{\eta}_k\mathbf{b}_1 + \phi_{k_y}\ddot{\eta}_k\mathbf{b}_2 + \phi_{k_z}\ddot{\eta}_k\mathbf{b}_3\right) \tag{10}$$

In the remaining text, Einstein notation is used when referring to the structural deformation. Terms having subscripts k are to be evaluated and summed from $k = 1$ to $k = M$, as in equations (8)–(10). For example, the last term in equation (10) is the acceleration component along the vertical body axis $\mathbf{b}_3$ due to structural deformation, and is written in this notation as

$$\sum_{k=1}^{M}\phi_{k_z}\ddot{\eta}_k \;=\; \phi_{1_z}\ddot{\eta}_1 + \phi_{2_z}\ddot{\eta}_2 + \ldots + \phi_{M_z}\ddot{\eta}_M \;\triangleq\; \phi_{k_z}\ddot{\eta}_k \tag{11}$$

This functional notation is introduced to simplify the expressions involving summations in the output measurement equations, and is similar to the shorthand typically used in flight dynamics literature to account for the effects of multiple control surface deflections [4].

A few points about the structural deformation model warrant further elaboration. First, note that the vibration modes describe the structural deformations when there is no air present, as in a vacuum. These vibratory modes are dependent upon the aircraft configuration, geometry, material properties, and mass properties. Analysis using a FEM and GVT data can determine the generalized masses, frequencies, and damping ratios of the vibration modes used in equation (7), as well the mode shapes for a sensor placed at an arbitrary location. These parameters may need to be scheduled using other parameters, such as fuel weight.

Second, it may seem inconsistent to use the vibration mode shapes, which are developed for when air is not present, to describe the aircraft motion when air is present. In flight, the frequencies and damping ratios of the aeroelastic vibrations change as a function of flight condition and dynamic pressure. However,

because the modal states pertain to these in-vacuo modes, this parameterization is a consistent and valid choice for parameterizing the deformation of the structure at any point on the aircraft, in space and time. Moreover, other basis functions could be used to describe the deformation, but the in-vacuo modes have physical significance for small displacements and can be measured and modeled using traditional methods.

Next, the structural deformations considered here are parameterized for small displacements, which can be approximated well by linear dynamic systems, as in equation (7). Analysis of these systems using eigenvalues and eigenvectors admits vibration modes which are mutually orthogonal with respect to the generalized mass matrix of the vibration modes [6]. Because the displacements are small, it is assumed that the aircraft mass properties, such as center of mass location or the inertia components, are not significantly affected. These assumptions are generally valid for conventional aircraft and normal flight conditions. For aircraft incurring large and nonlinear deformations, such as HALE-type aircraft [13, 14], more complex structural deformation models may be required. The equations presented in this report are still valid in this case, but the parameterization for the structural deformation $\mathbf{r}^{CD}$ would need to be revised.

Lastly, consider the relative magnitudes of the modal displacements, rates, and accelerations. The steady-state response of the i^{th} mode to a sinusoidal input at its natural frequency is

$$\eta_i = a_i \sin(\omega_i t + \phi_i) \tag{12a}$$

The modal rate and acceleration are then

$$\dot{\eta}_i = a_i \, \omega_i \cos(\omega_i t + \phi_i) \tag{12b}$$

$$\ddot{\eta}_i = -a_i \, \omega_i^2 \sin(\omega_i t + \phi_i) \tag{12c}$$

The relative amplitudes of the modal displacement, rates, and acceleration are therefore 1, ω_i, and ω_i^2. Variations of these relative amplitudes with frequency are shown in figure 7. For natural frequencies greater than 1 rad/s (or about 0.16 Hz), which is usually the case with aircraft vibration modes, the modal displacements, rates, and accelerations can be orders of magnitude different. This observation will be used later in this report as justification for neglecting lower derivatives of η to simplify the output measurement equations.

Conventional Forms

The vector definitions and structural deformation model developed are now written using conventional aircraft nomenclature [3, 4] and scalar equations. The aircraft inertial attitude is parameterized using the conventional yaw-pitch-roll sequence of Euler angles used in flight dynamics [4], in which rotation from an inertial frame to the body frame undergoes first a yaw rotation through ψ, then a pitch rotation through θ, and finally a roll rotation through ϕ. The angular velocity and angular acceleration of the mean axes are

$$\boldsymbol{\omega} = p \, \mathbf{b}_1 + q \, \mathbf{b}_2 + r \, \mathbf{b}_3 \tag{13}$$

$$\boldsymbol{\alpha} = \dot{p} \, \mathbf{b}_1 + \dot{q} \, \mathbf{b}_2 + \dot{r} \, \mathbf{b}_3 \tag{14}$$

The aircraft mass center $B^\star$ has inertial position, velocity, and acceleration

$$\mathbf{r}^{OB^\star} = x \, \mathbf{n}_1 + y \, \mathbf{n}_2 + z \, \mathbf{n}_3 \tag{15}$$

$${}^N\mathbf{v}^{B^\star} = u \, \mathbf{b}_1 + v \, \mathbf{b}_2 + w \, \mathbf{b}_3 \tag{16}$$

$${}^N\mathbf{a}^{B^\star} = (\dot{u} + qw - rv)\mathbf{b}_1 + (\dot{v} + ru - pw)\mathbf{b}_2 + (\dot{w} + pv - qu)\mathbf{b}_3 \tag{17}$$

Instead of using the mean-axis velocity components u, v, and w, the velocity of the aircraft mass center

could be parameterized using the stability axes or wind axes, as illustrated in figure 8, where

$$V = \sqrt{u^2 + v^2 + w^2} \tag{18}$$

$$\alpha = \arctan\left(\frac{w}{u}\right) \tag{19}$$

$$\beta = \arcsin\left(\frac{v}{V}\right) \tag{20}$$

$$\mu = \arctan\left(\frac{v}{u}\right) \tag{21}$$

are the true airspeed, angle of attack, angle of sideslip, and flank angle at the mass center.

The installed sensor location at point C has position fixed in the mean axes

$$\mathbf{r}^{B^*C} = x_s\,\mathbf{b}_1 + y_s\,\mathbf{b}_2 + z_s\,\mathbf{b}_3 \tag{22}$$

The sensor location, when deformed from C to D, has the inertial position and velocity

$$\mathbf{r}^{OD} = x_D\,\mathbf{n}_1 + y_D\,\mathbf{n}_2 + z_D\,\mathbf{n}_3 \tag{23}$$

$${}^N\mathbf{v}^D = u_D\,\mathbf{b}_1 + v_D\,\mathbf{b}_2 + w_D\,\mathbf{b}_3 \tag{24}$$

Substituting the developed scalar quantities into equation (1), expanding the equations, and writing the terms in the inertial frame, the position of the sensor at D is

$$\begin{aligned} x_D = {} & x + (\cos\theta\cos\psi)\,(x_s + \phi_{k_x}\eta_k) + (\sin\phi\sin\theta\cos\psi - \cos\phi\sin\psi)\,\left(y_s + \phi_{k_y}\eta_k\right) \\ & + (\cos\phi\sin\theta\cos\psi + \sin\phi\sin\psi)\,(z_s + \phi_{k_z}\eta_k) \end{aligned} \tag{25a}$$

$$\begin{aligned} y_D = {} & y + (\cos\theta\sin\psi)\,(x_s + \phi_{k_x}\eta_k) + (\sin\phi\sin\theta\sin\psi + \cos\phi\cos\psi)\,\left(y_s + \phi_{k_y}\eta_k\right) \\ & + (\cos\phi\sin\theta\sin\psi - \sin\phi\cos\psi)\,(z_s + \phi_{k_z}\eta_k) \end{aligned} \tag{25b}$$

$$\begin{aligned} z_D = {} & z - (\sin\theta)\,(x_s + \phi_{k_x}\eta_k) + (\sin\phi\cos\theta)\,\left(y_s + \phi_{k_y}\eta_k\right) \\ & + (\cos\phi\cos\theta)\,(z_s + \phi_{k_z}\eta_k) \end{aligned} \tag{25c}$$

Similarly, substituting the developed scalar quantities into equation (2) and writing in terms of the body frame yields the velocity components at point D as

$$u_D = u - r(y_s + \phi_{k_y}\eta_k) + q(z_s + \phi_{k_z}\eta_k) + \phi_{k_x}\dot{\eta}_k \tag{26a}$$

$$v_D = v + r(x_s + \phi_{k_x}\eta_k) - p(z_s + \phi_{k_z}\eta_k) + \phi_{k_y}\dot{\eta}_k \tag{26b}$$

$$w_D = w - q(x_s + \phi_{k_x}\eta_k) + p(y_s + \phi_{k_y}\eta_k) + \phi_{k_z}\dot{\eta}_k \tag{26c}$$

4 Output Measurement Equations

This section discusses the output measurement equations for sensors commonly installed on a flexible aircraft. Equations are first presented in full form, and then simplifications are applied to reduce and linearize the equations, where appropriate. The emphasis is on the contributions of the aircraft flexibility to the measurements, so other important effects such as measurement noise, bias and scale factor errors, transducer dynamics, time delays, cross-talk, misalignment, etc., are not mentioned but are discussed in other works, such as references [1–3, 15, 16]. For illustrative purposes, the X-56A flight test data shown in figures 3–4 are again referenced.

Each sensor is assumed to be installed at point C and located at point D when undergoing structural deformation. The mode shapes ϕ_{k_x}, ϕ_{k_y}, and ϕ_{k_z} and the installed position of the sensor x_s, y_s, and z_s correspond to the sensor in question. When performing flight dynamics work that involves multiple sensors, additional notation is required to distinguish between different sensors.

Linear Accelerometers

One of the most important sensors for observing aeroelastic effects on a flexible aircraft is a linear accelerometer, due in part to the high bandwidth and sensitivity of the sensor. Linear accelerometers measure the translational acceleration due to applied forces, excluding gravity [3, 16]. A derivation of the accelerometer outputs using vector notation is provided in appendix A, where two different but equivalent forms for the outputs are developed. These forms, expanded as scalar equations, are discussed sequentially in this section.

A sensor containing a collocated triad of accelerometers at point D has the output

$$\boldsymbol{a}_D = a_{x_D}\mathbf{b}_1 + a_{y_D}\mathbf{b}_2 + a_{z_D}\mathbf{b}_3 \tag{27}$$

where a_{x_D}, a_{y_D}, and a_{z_D} are the components in the body axes. Note $\boldsymbol{a}$ is the accelerometer output whereas $\mathbf{a}$ is the kinematic acceleration. Some accelerometers give only one component of this measurement rather than all three components.

The first form for the accelerometer outputs is written in terms of the specific applied forces, as follows from substituting equation (A-7a) into equation (A-8). Expanding this vector equation using scalar notation, the outputs are

$$\begin{aligned} g\,a_{x_D} = {} & \frac{\bar{q}SC_X + X_p}{m} - \left(q^2 + r^2\right)\left(x_s + \phi_{k_x}\eta_k\right) + \left(pq - \dot{r}\right)\left(y_s + \phi_{k_y}\eta_k\right) \\ & + \left(pr + \dot{q}\right)\left(z_s + \phi_{k_z}\eta_k\right) + 2\left(\phi_{k_z}q - \phi_{k_y}r\right)\dot{\eta}_k + \phi_{k_x}\ddot{\eta}_k \end{aligned} \tag{28a}$$

$$\begin{aligned} g\,a_{y_D} = {} & \frac{\bar{q}SC_Y + Y_p}{m} + \left(pq + \dot{r}\right)\left(x_s + \phi_{k_x}\eta_k\right) - \left(p^2 + r^2\right)\left(y_s + \phi_{k_y}\eta_k\right) \\ & + \left(qr - \dot{p}\right)\left(z_s + \phi_{k_z}\eta_k\right) + 2\left(\phi_{k_x}r - \phi_{k_z}p\right)\dot{\eta}_k + \phi_{k_y}\ddot{\eta}_k \end{aligned} \tag{28b}$$

$$\begin{aligned} g\,a_{z_D} = {} & \frac{\bar{q}SC_Z + Z_p}{m} + \left(pr - \dot{q}\right)\left(x_s + \phi_{k_x}\eta_k\right) + \left(qr + \dot{p}\right)\left(y_s + \phi_{k_y}\eta_k\right) \\ & - \left(p^2 + q^2\right)\left(z_s + \phi_{k_z}\eta_k\right) + 2\left(\phi_{k_y}p - \phi_{k_x}q\right)\dot{\eta}_k + \phi_{k_z}\ddot{\eta}_k \end{aligned} \tag{28c}$$

The accelerometer outputs a_{x_D}, a_{y_D}, and a_{z_D} are typically given in g units; however, the g factor has been moved to the left side of the equations in this report, for convenience. The terms C_X, C_Y, and C_Z are the nondimensional aerodynamic force coefficients along the body axes, and X_p, Y_p, and Z_p are the propulsive forces. The aerodynamic forces could instead be written in the stability axes using C_D and C_L

by substituting

$$C_X = -C_D \cos\alpha + C_L \sin\alpha \tag{29a}$$

$$C_Z = -C_D \sin\alpha - C_L \cos\alpha \tag{29b}$$

in equations (28a)–(28c).

To simplify these accelerometer outputs, the contributions from η and $\dot{\eta}$ can often be neglected for vibration modes with natural frequencies above 1 rad/s, as discussed in section 3. In addition, the propulsive thrust vector is often aligned with $\mathbf{b}_1$ so that $Y_p = Z_p = 0$. These simplifications reduce the accelerometer outputs to

$$g\, a_{x_D} = \frac{\bar{q}SC_X + X_p}{m} - \left(q^2 + r^2\right) x_s + (pq - \dot{r})\, y_s + (pr + \dot{q})\, z_s + \phi_{k_x} \ddot{\eta}_k \tag{30a}$$

$$g\, a_{y_D} = \frac{\bar{q}SC_Y}{m} + (pq + \dot{r})\, x_s - \left(p^2 + r^2\right) y_s + (qr - \dot{p})\, z_s + \phi_{k_y} \ddot{\eta}_k \tag{30b}$$

$$g\, a_{z_D} = \frac{\bar{q}SC_Z}{m} + (pr - \dot{q})\, x_s + (qr + \dot{p})\, y_s - \left(p^2 + q^2\right) z_s + \phi_{k_z} \ddot{\eta}_k \tag{30c}$$

These equations are the same for accelerometer outputs on a rigid aircraft [1, 3], except for the additional modal acceleration terms at the end of these equations.

Another way to simplify these equations is to linearize them about a reference flight condition. Using the procedure described in reference [17], the linearized versions of equations (28a)–(28c) are

$$\begin{aligned} g\, \Delta a_{x_D} = {} & \frac{\bar{q}_0 S}{m_0} \Delta C_X + \frac{2\bar{q}_0 S\, C_{X_0}}{m_0 V_0} \Delta V + \frac{\Delta X_p}{m_0} \\ & + (z_s + \phi_{k_z} \eta_{k_0})\, \Delta\dot{q} - \left(y_s + \phi_{k_y} \eta_{k_0}\right) \Delta\dot{r} + \phi_{k_x} \Delta\ddot{\eta}_k \end{aligned} \tag{31a}$$

$$\begin{aligned} g\, \Delta a_{y_D} = {} & \frac{\bar{q}_0 S}{m_0} \Delta C_Y + \frac{2\bar{q}_0 S\, C_{Y_0}}{m_0 V_0} \Delta V + \frac{\Delta Y_p}{m_0} \\ & - (z_s + \phi_{k_z} \eta_{k_0})\, \Delta\dot{p} + (x_s + \phi_{k_x} \eta_{k_0})\, \Delta\dot{r} + \phi_{k_y} \Delta\ddot{\eta}_k \end{aligned} \tag{31b}$$

$$\begin{aligned} g\, \Delta a_{z_D} = {} & \frac{\bar{q}_0 S}{m_0} \Delta C_Z + \frac{2\bar{q}_0 S\, C_{Z_0}}{m_0 V_0} \Delta V + \frac{\Delta Z_p}{m_0} \\ & + \left(y_s + \phi_{k_y} \eta_{k_0}\right) \Delta\dot{p} - (x_s + \phi_{k_x} \eta_{k_0})\, \Delta\dot{q} + \phi_{k_z} \Delta\ddot{\eta}_k \end{aligned} \tag{31c}$$

where the 0 subscript indicates a reference value about which the linearization is performed, and where the Δ symbol denotes a perturbation value, e.g.,

$$C_Z = C_{Z_0} + \Delta C_Z \tag{32}$$

The ΔV terms in equations (31a)–(31c) arise from variations in dynamic pressure and, along with perturbations in the propulsive forces, can often be neglected in many maneuvers. The aircraft mass and wing reference area were assumed to be constant in these linearizations. If the stability-axis force coefficients are

used instead of the body-axis coefficients, the linearized equations are

$$\begin{aligned} g\,\Delta a_{x_D} = {} & \frac{\bar{q}_0 S}{m_0}\left(-\Delta C_D \cos\alpha_0 + \Delta C_L \sin\alpha_0\right) + \frac{2\bar{q}_0 S}{m_0 V_0}\left(-C_{D_0}\cos\alpha_0 + C_{L_0}\sin\alpha_0\right)\Delta V \\ & \frac{\bar{q}_0 S}{m_0}\left(C_{D_0}\sin\alpha_0 + C_{L_0}\cos\alpha_0\right)\Delta\alpha + \frac{\Delta X_p}{m_0} \\ & + \left(z_s + \phi_{k_z}\eta_{k_0}\right)\Delta\dot{q} - \left(y_s + \phi_{k_y}\eta_{k_0}\right)\Delta\dot{r} + \phi_{k_x}\Delta\ddot{\eta}_k \end{aligned} \tag{33a}$$

$$\begin{aligned} g\,\Delta a_{y_D} = {} & \frac{\bar{q}_0 S}{m_0}\Delta C_Y + \frac{2\bar{q}_0 S\, C_{Y_0}}{m_0 V_0}\Delta V + \frac{\Delta Y_p}{m_0} \\ & - \left(z_s + \phi_{k_z}\eta_{k_0}\right)\Delta\dot{p} + \left(x_s + \phi_{k_x}\eta_{k_0}\right)\Delta\dot{r} + \phi_{k_y}\Delta\ddot{\eta}_k \end{aligned} \tag{33b}$$

$$\begin{aligned} g\,\Delta a_{z_D} = {} & \frac{\bar{q}_0 S}{m_0}\left(-\Delta C_D \sin\alpha_0 - \Delta C_L \cos\alpha_0\right) + \frac{2\bar{q}_0 S}{m_0 V_0}\left(-C_{D_0}\sin\alpha_0 - C_{L_0}\cos\alpha_0\right)\Delta V \\ & + \frac{\bar{q}_0 S}{m_0}\left(-C_{D_0}\cos\alpha_0 + C_{L_0}\sin\alpha_0\right)\Delta\alpha + \frac{\Delta Z_p}{m_0} \\ & + \left(y_s + \phi_{k_y}\eta_{k_0}\right)\Delta\dot{p} - \left(x_s + \phi_{k_x}\eta_{k_0}\right)\Delta\dot{q} + \phi_{k_z}\Delta\ddot{\eta}_k \end{aligned} \tag{33c}$$

in which both C_D and C_L affect Δa_{x_D} and Δa_{z_D}. The additional $\Delta\alpha$ terms are due to the rotation from body frame to stability frame. The equation for the lateral accelerometer output is unchanged from before.

Equations (31a)–(33c) are linear in the states and controls of the aircraft, and can be assembled into transfer function models or into the output equations for state-space models. In many cases the static deformation of the structure η_{k_0} can be neglected. However, in some conditions, such as during high wing loads or in high-g turns, the effects of the static deformations may be significant.

The second form for the accelerometer output is written in terms of the aircraft states and their derivatives, which follows from substituting equation (A-7b) into equation (A-8). Expanding this vector equation using scalar notation, the outputs are

$$\begin{aligned} g\,a_{x_D} = {} & \dot{u} + q\left(w + 2\phi_{k_z}\dot{\eta}_k\right) - r\left(v + 2\phi_{k_y}\dot{\eta}_k\right) + g\sin\theta \\ & - \left(q^2 + r^2\right)\left(x_s + \phi_{k_x}\eta_k\right) + \left(pq - \dot{r}\right)\left(y_s + \phi_{k_y}\eta_k\right) \\ & + \left(pr + \dot{q}\right)\left(z_s + \phi_{k_z}\eta_k\right) + \phi_{k_x}\ddot{\eta}_k \end{aligned} \tag{34a}$$

$$\begin{aligned} g\,a_{y_D} = {} & \dot{v} + r\left(u + 2\phi_{k_x}\dot{\eta}_k\right) - p\left(w + 2\phi_{k_z}\dot{\eta}_k\right) - g\sin\phi\cos\theta \\ & + \left(pq + \dot{r}\right)\left(x_s + \phi_{k_x}\eta_k\right) - \left(p^2 + r^2\right)\left(y_s + \phi_{k_y}\eta_k\right) \\ & + \left(qr - \dot{p}\right)\left(z_s + \phi_{k_z}\eta_k\right) + \phi_{k_y}\ddot{\eta}_k \end{aligned} \tag{34b}$$

$$\begin{aligned} g\,a_{z_D} = {} & \dot{w} + p\left(v + 2\phi_{k_y}\dot{\eta}_k\right) - q\left(u + 2\phi_{k_x}\dot{\eta}_k\right) - g\cos\phi\cos\theta \\ & + \left(pr - \dot{q}\right)\left(x_s + \phi_{k_x}\eta_k\right) + \left(qr + \dot{p}\right)\left(y_s + \phi_{k_y}\eta_k\right) \\ & - \left(p^2 + q^2\right)\left(z_s + \phi_{k_z}\eta_k\right) + \phi_{k_z}\ddot{\eta}_k \end{aligned} \tag{34c}$$

To simplify these accelerometer outputs, η and $\dot{\eta}$ could be neglected, as before, resulting in

$$\begin{aligned} g\, a_{x_D} &= \dot{u} + qw - rv + g\sin\theta \\ &\quad - \left(q^2 + r^2\right) x_s + (pq - \dot{r})\, y_s + (pr + \dot{q})\, z_s + \phi_{k_x} \ddot{\eta}_k \end{aligned} \tag{35a}$$

$$\begin{aligned} g\, a_{y_D} &= \dot{v} + ru - pw - g\sin\phi\cos\theta \\ &\quad + (pq + \dot{r})\, x_s - \left(p^2 + r^2\right) y_s + (qr - \dot{p})\, z_s + \phi_{k_y} \ddot{\eta}_k \end{aligned} \tag{35b}$$

$$\begin{aligned} g\, a_{z_D} &= \dot{w} + pv - qu - g\cos\phi\cos\theta \\ &\quad + (pr - \dot{q})\, x_s + (qr + \dot{p})\, y_s - \left(p^2 + q^2\right) z_s + \phi_{k_z} \ddot{\eta}_k \end{aligned} \tag{35c}$$

which, again, are the standard output equations for rigid aircraft but with additional contributions due to the modal accelerations. Linearizing equations (34a)–(34c) about a reference condition using velocities in the body axes yields

$$\begin{aligned} g\, \Delta a_{x_D} &= \Delta\dot{u} + w_0 \Delta q - v_0 \Delta r + (g\cos\theta)\, \Delta\theta \\ &\quad + (z_s + \phi_{k_z}\eta_{k_0})\, \Delta\dot{q} - \left(y_s + \phi_{k_y}\eta_{k_0}\right) \Delta\dot{r} + \phi_{k_x} \Delta\ddot{\eta}_k \end{aligned} \tag{36a}$$

$$\begin{aligned} g\, \Delta a_{y_D} &= \Delta\dot{v} - w_0 \Delta p + u_0 \Delta r - (g\cos\phi_0\cos\theta_0)\, \Delta\phi + (g\sin\phi_0\sin\theta_0)\, \Delta\theta \\ &\quad - (z_s + \phi_{k_z}\eta_{k_0})\, \Delta\dot{p} + (x_s + \phi_{k_x}\eta_{k_0})\, \Delta\dot{r} + \phi_{k_y} \Delta\ddot{\eta}_k \end{aligned} \tag{36b}$$

$$\begin{aligned} g\, \Delta a_{z_D} &= \Delta\dot{w} + v_0 \Delta p - u_0 \Delta q + (g\sin\phi_0\cos\theta_0)\, \Delta\phi + (g\cos\phi_0\sin\theta_0)\, \Delta\theta \\ &\quad + \left(y_s + \phi_{k_y}\eta_{k_0}\right) \Delta\dot{p} - (x_s - \phi_{k_x}\eta_{k_0})\, \Delta\dot{q} + \phi_{k_z} \Delta\ddot{\eta}_k \end{aligned} \tag{36c}$$

or, if the stability axes are used, yields

$$\begin{aligned} g\, \Delta a_{x_D} &= (\cos\alpha_0\cos\beta_0)\, \Delta\dot{V} + (-V_0\cos\alpha_0\cos\beta_0)\, \Delta\dot{\beta} + (-V_0\sin\alpha_0\cos\beta_0)\, \Delta\dot{\alpha} \\ &\quad + (V_0\sin\alpha_0\cos\beta_0)\, \Delta q + (-V_0\sin\beta_0)\, \Delta r + (g\cos\theta)\, \Delta\theta \\ &\quad + (z_s + \phi_{k_z}\eta_{k_0})\, \Delta\dot{q} - \left(y_s + \phi_{k_y}\eta_{k_0}\right) \Delta\dot{r} + \phi_{k_x} \Delta\ddot{\eta}_k \end{aligned} \tag{37a}$$

$$\begin{aligned} g\, \Delta a_{y_D} &= (\sin\beta_0)\, \Delta\dot{V} + (V_0\cos\beta_0)\, \Delta\dot{\beta} + (-V_0\sin\alpha_0\cos\beta_0)\, \Delta p \\ &\quad + (V_0\cos\alpha_0\cos\beta_0)\, \Delta r + (-g\cos\phi_0\cos\theta_0)\, \Delta\phi + (g\sin\phi_0\sin\theta_0)\, \Delta\theta \\ &\quad - (z_s + \phi_{k_z}\eta_{k_0})\, \Delta\dot{p} + (x_s + \phi_{k_x}\eta_{k_0})\, \Delta\dot{r} + \phi_{k_y} \Delta\ddot{\eta}_k \end{aligned} \tag{37b}$$

$$\begin{aligned} g\, \Delta a_{z_D} &= (\sin\alpha_0\cos\beta_0)\, \Delta\dot{V} + (-V_0\sin\alpha_0\sin\beta_0)\, \Delta\dot{\beta} + (V_0\cos\alpha_0\cos\beta_0)\, \Delta\dot{\alpha} \\ &\quad + (g\sin\phi_0\cos\theta_0)\, \Delta\phi + (g\cos\phi_0\sin\theta_0)\, \Delta\theta \\ &\quad + \left(y_s + \phi_{k_y}\eta_{k_0}\right) \Delta\dot{p} - (x_s - \phi_{k_x}\eta_{k_0})\, \Delta\dot{q} + \phi_{k_z} \Delta\ddot{\eta}_k \end{aligned} \tag{37c}$$

The X-56A flight test data for a_z shown in figures 3–4 is from a vertical accelerometer placed on the left wing, near the leading edge of the wingtip. As with all sensors, the installation location determines which modes are observable in the measurements. For example, an accelerometer placed at a node of a particular vibration mode will not have any contributions to the output from that mode. Frequency content from the short period mode is present because of the contribution from $\Delta\dot{q}$ and because that mode depends on lift generation through C_Z or C_L. Content from the SW1B mode is present because the accelerometer is placed near the wingtip, where ϕ_{7_z} is large. Lastly, content from the SW1T mode is present because the sensor is located forward of the elastic axis of the wing and ϕ_{9_z} is large. Figure 5 gives an idea of the relative size of ϕ_{k_z} for the SW1B and SW1T modes.

Strain Gauges

Another important sensor for flexible aircraft dynamics is the strain gauge, which measures normalized deformations of the local structure. The measurements are sensitive to a particular axis or type of strain depending on the sensor type, configuration, and orientation. Fiber-optic strain sensors, which can provide many strain measurements along the distributed sensing aperture, are also becoming common in flight tests [18]. Similar to accelerometers, strain sensors have wide bandwidth and give useful information on the vibration modes. In contrast to accelerometers, this information is on the generalized modal displacements rather than the modal accelerations. Strain outputs are relatively simple in that only the modal displacements contribute to the output, whereas accelerometers have contributions from many sources.

The strains measured are typically small and within the range of elastic deformation. As such, the measurement equations for strain sensors are typically written as

$$\epsilon_D = \psi_k \eta_k \tag{38}$$

which is already in a linear form. The strain modes ψ_k are the strains registered by the sensor due to a unit displacement in η_k, and can be obtained from a FEM or GVT data, such as in figure 5. If temperature compensation is not implemented in the hardware, additional terms are needed for this calibration.

The strain gauge data shown in figures 3–4 was measured with a bending strain gauge attached near the root of the right wing. Content from the short period and SW1B modes are present in the data. The SW1T mode is also present, but to a lesser extent because that mode only contains a small amount of wing bending at the wing root, resulting in a low value of ψ_9.

Rate Gyroscopes

Rate gyroscopes measure the angular rate components of the aircraft. The output equations consist of the mean-axes angular rate and the local angular rate due to angular deformation of the aircraft structure. The gyroscope output equations are

$$p_D = p + \nu_{k_\phi} \dot{\eta}_k \tag{39a}$$

$$q_D = q + \nu_{k_\theta} \dot{\eta}_k \tag{39b}$$

$$r_D = r + \nu_{k_\psi} \dot{\eta}_k \tag{39c}$$

where ν_{k_ϕ}, ν_{k_θ}, and ν_{k_ψ} are the angular displacements from C to D incurred by a unit displacement of η_k. These terms, sometimes called the modal slopes, can be obtained by computing local derivatives of the mode shapes with respect to the spatial dimensions, such as from figure 5. The angular rate output equations are already in linear form and can be directly assembled into a state-space or transfer function model.

For the sample flight test data in figures 3–4, the pitch rate data was from a gyroscope installed near the nose along the centerline. The short period and SW1B modes were present in this measurement, with negligible amplitudes from the SW1T mode. This was because the gyroscopes were installed near the aircraft nose where, as illustrated in figure 5, there is bending from the SW1B mode but little torsion from the SW1T mode, resulting in a large ν_{7_θ} and small ν_{9_θ}.

Angular Accelerometers

Angular accelerometers are seldom used in flight testing; rather, this information is more often obtained from numerical differentiation of measured angular rate data [3]. Regardless, the corresponding output equations for this data are

$$\dot{p}_D = \dot{p} + \nu_{k_\phi} \ddot{\eta}_k \tag{40a}$$

$$\dot{q}_D = \dot{q} + \nu_{k_\theta} \ddot{\eta}_k \tag{40b}$$

$$\dot{r}_D = \dot{r} + \nu_{k_\psi} \ddot{\eta}_k \tag{40c}$$

which is a combination of the mean-axis angular accelerations and the local angular accelerations of the aircraft structure. These equations come from differentiating equations (39a)–(39c) with respect to time, and are already in a linear form.

The pitch acceleration data shown in figures 3–4 was obtained by differentiating measured pitch rate data in the frequency domain. Due to this dependence, the angular acceleration data exhibited the same modal components as the angular rate data previously mentioned. Specifically, there were significant content from the short period and SW1B modes, but little content from the SW1T mode.

Euler Angles

The Euler angles describing the aircraft attitude are estimated from sensor data, and are usually the output of an inertial measurement unit or inertial navigation system onboard the aircraft. For traditional rigid aircraft, the attitude estimate is essentially the solution to the differential equations

$$\dot{\phi} = p + q \sin\phi \tan\theta + r \cos\phi \tan\theta \tag{41a}$$

$$\dot{\theta} = q \cos\phi - r \sin\phi \tag{41b}$$

$$\dot{\psi} = q \sin\phi \sec\theta + r \cos\phi \sec\theta \tag{41c}$$

using measured angular rate data. In addition, data from magnetometers, accelerometers, airdata probes, and other sensors can be combined in an extended Kalman filter to improve the attitude estimate.

If this type of attitude estimation is used for flexible aircraft, a closed-form solution to the estimated Euler angle outputs is not possible. If vibration mode states can be estimated and their effects removed from the sensor data [19], traditional attitude estimation techniques can still be applied. Otherwise, the flexibility effects become confounded in the estimated attitude output as a function of which sensor data is included in the estimation, the local mode shapes for each of the sensors, the measurement and process noise covariance matrices selected, filters internal to the sensor package, and other factors.

If the relevant sensors are installed close enough together on the aircraft that they may be assumed to be collocated at a single point, equations (41a)–(41c) are approximately

$$\dot{\phi}_D = (p + \nu_{k_\phi} \dot{\eta}_k) + (q + \nu_{k_\theta} \dot{\eta}_k) \sin\phi_D \tan\theta_D + (r + \nu_{k_\psi} \dot{\eta}_k) \cos\phi_D \tan\theta_D \tag{42a}$$

$$\dot{\theta}_D = (q + \nu_{k_\theta} \dot{\eta}_k) \cos\phi_D - (r + \nu_{k_\psi} \dot{\eta}_k) \sin\phi_D \tag{42b}$$

$$\dot{\psi}_D = (q + \nu_{k_\theta} \dot{\eta}_k) \sin\phi_D \sec\theta_D + (r + \nu_{k_\psi} \dot{\eta}_k) \cos\phi_D \sec\theta_D \tag{42c}$$

Linearizing this differential equation about a reference condition results in

$$\begin{aligned}\Delta\dot{\phi}_D = {} & \Delta p + (\sin\phi_{D_0}\tan\theta_{D_0})\,\Delta q + (\cos\phi_{D_0}\tan\theta_{D_0})\,\Delta r \\ & + \left(\nu_{k_\phi} + \nu_{k_\theta}\sin\phi_{D_0}\tan\theta_{D_0} + \nu_{k_\psi}\cos\phi_{D_0}\tan\theta_{D_0}\right)\Delta\dot{\eta}_k \end{aligned} \tag{43a}$$

$$\Delta\dot{\theta}_D = (\cos\theta_{D_0})\,\Delta q - (\sin\phi_{D_0})\,\Delta r + \left(\nu_{k_\theta}\cos\theta_{D_0} - \nu_{k_\psi}\sin\phi_{D_0}\right)\Delta\dot{\eta}_k \tag{43b}$$

$$\begin{aligned}\Delta\dot{\psi}_D = {} & (\sin\phi_{D_0}\sec\theta_{D_0})\,\Delta q + (\cos\phi_{D_0}\sec\theta_{D_0})\,\Delta r \\ & + \left(\nu_{k_\theta}\sin\phi_{D_0}\sec\theta_{D_0} + \nu_{k_\psi}\cos\phi_{D_0}\sec\theta_{D_0}\right)\Delta\dot{\eta}_k \end{aligned} \tag{43c}$$

For small ϕ_{D_0} and θ_{D_0}, such as in steady wings-level flight, these equations may be approximated as

$$\Delta\dot{\phi}_D = \Delta p + \nu_{k_\phi}\Delta\dot{\eta}_k \tag{44a}$$

$$\Delta\dot{\theta}_D = \Delta q + \nu_{k_\theta}\Delta\dot{\eta}_k \tag{44b}$$

$$\Delta\dot{\psi}_D = \Delta r + \nu_{k_\psi}\Delta\dot{\eta}_k \tag{44c}$$

which have the solutions

$$\Delta\phi_D = \Delta\phi + \nu_{k_\phi}\Delta\eta_k \tag{45a}$$

$$\Delta\theta_D = \Delta\theta + \nu_{k_\theta}\Delta\eta_k \tag{45b}$$

$$\Delta\psi_D = \Delta\psi + \nu_{k_\psi}\Delta\eta_k \tag{45c}$$

Adding these perturbation solutions to the initial conditions, the approximate outputs of the attitude solution using Euler angles is

$$\phi_D = \phi + \nu_{k_\phi}\eta_k \tag{46a}$$

$$\theta_D = \theta + \nu_{k_\theta}\eta_k \tag{46b}$$

$$\psi_D = \psi + \nu_{k_\psi}\eta_k \tag{46c}$$

Equations (44a)–(44c) are similar to the differential equations typically used in linearized models of rigid-body flight dynamics [3, 4], except these equations include additional terms due to the modal rates. The solutions to these equations, given as equations (45a)–(45c), show that the Euler angle outputs are primarily a combination of the body mean-axis Euler angles and the local rotational deformations of the aircraft structure.

In the flight test data shown in figures 3–4, the pitch angle data was taken from an inertial navigation system located near the aircraft mass center. The largest amplitudes are due to the short period response of the airplane. The SW1B mode, and to a much lesser extent also the SW1T mode, were also present in the measurement, similar to the angular rate data. Differentiated Euler angle data matched the measured gyroscope data well over the bandwidth of the short period mode. However, the content near the SW1B and SW1T modes did not match because the values of ν_{7_θ} and ν_{9_θ} were different for the two sensor locations.

Airspeed

True airspeed is often computed from dynamic pressure measurements and other data for subsonic flight. The (squared, for convenience) airspeed measurement can be written in terms of the velocities at D from equations (26a)–(26c) as

$$\begin{aligned} V_D^2 &= u_D^2 + v_D^2 + w_D^2 \\ &= \left[u - r(y_s + \phi_{k_y}\eta_k) + q(z_s + \phi_{k_z}\eta_k) + \phi_{k_x}\dot{\eta}_k\right]^2 \\ &\quad + \left[v + r(x_s + \phi_{k_x}\eta_k) - p(z_s + \phi_{k_z}\eta_k) + \phi_{k_y}\dot{\eta}_k\right]^2 \\ &\quad + \left[w - q(x_s + \phi_{k_x}\eta_k) + p(y_s + \phi_{k_y}\eta_k) + \phi_{k_z}\dot{\eta}_k\right]^2 \end{aligned} \tag{47}$$

These equations, as well as those developed next for angle of attack and sideslip or flank angle, account only for the inertial velocity of the aircraft and do not consider effects of a moving atmosphere or how the flow immediately surrounding the aircraft is disturbed relative to the freestream.

In many cases, this equation can be simplified by neglecting η, which should be much smaller than $\dot{\eta}$. Further simplification can occur when airdata booms extend from the nose or wing tips, in which y_s and/or z_s are small. For full-scale aircraft, contributions from the angular rates may be negligible. The modal rates $\dot{\eta}$ may also have little effect on the output measurement.

Linearizing the airspeed measurement about a reference condition using the mean axes results in

$$\begin{aligned} \Delta V_D = &\left[\frac{u_0}{\sqrt{u_0^2 + v_0^2 + w_0^2}}\right]\Delta u + \left[\frac{v_0}{\sqrt{u_0^2 + v_0^2 + w_0^2}}\right]\Delta v + \left[\frac{w_0}{\sqrt{u_0^2 + v_0^2 + w_0^2}}\right]\Delta w \\ &+ \left[\frac{w_0(y_s + \phi_{y_k}\eta_{k_0}) - v_0(z_s + \phi_{z_k}\eta_{k_0})}{\sqrt{u_0^2 + v_0^2 + w_0^2}}\right]\Delta p \\ &+ \left[\frac{u_0(z_s + \phi_{z_k}\eta_{k_0}) - w_0(x_s + \phi_{x_k}\eta_{k_0})}{\sqrt{u_0^2 + v_0^2 + w_0^2}}\right]\Delta q \\ &+ \left[\frac{v_0(x_s + \phi_{x_k}\eta_{k_0}) - u_0(y_s + \phi_{y_k}\eta_{k_0})}{\sqrt{u_0^2 + v_0^2 + w_0^2}}\right]\Delta r + \left[\frac{u_0\phi_{k_x} + v_0\phi_{k_y} + w_0\phi_{k_z}}{\sqrt{u_0^2 + v_0^2 + w_0^2}}\right]\Delta\dot{\eta}_k \end{aligned} \tag{48}$$

or, using the stability axes,

$$\begin{aligned} \Delta V_D = \Delta V &+ \left[\sin\alpha_0\cos\beta_0(y_s + \phi_{k_y}\eta_{k_0}) - \sin\beta_0(z_s + \phi_{k_z}\eta_{k_0})\right]\Delta p \\ &+ \left[\cos\alpha_0\cos\beta_0(z_s + \phi_{k_z}\eta_{k_0}) - \sin\alpha_0\cos\beta_0(x_s + \phi_{k_x}\eta_{k_0})\right]\Delta q \\ &+ \left[\sin\beta_0(x_s + \phi_{k_x}\eta_{k_0}) - \cos\alpha_0\cos\beta_0(y_s + \phi_{k_y}\eta_{k_0})\right]\Delta r \\ &+ \left[\phi_{k_x}\cos\alpha_0\cos\beta_0 + \phi_{k_y}\sin\beta_0 + \phi_{k_z}\sin\alpha_0\cos\beta_0\right]\Delta\dot{\eta}_k \end{aligned} \tag{49}$$

The dominant term in these linearized forms is the forward speed or true airspeed, with smaller contributions from the angular rates and the modal rates. In general, the linearization for airspeed, and also for angle of attack and sideslip or flank angle, has a larger range of validity when using stability-axis velocities because the outputs involve a lesser degree of nonlinearity than when body-axis velocities are used.

The airdata measurements shown in figures 3–4 used a NACA probe protruding from the aircraft nose. The measurements had only low-frequency content, near the phugoid mode and short period mode, and were not significantly affected by structural deformations during this maneuver. Quantities with relatively low-frequency content, such as airspeed and dynamic pressure, are less sensitive to structural vibrations of the

aircraft, which generally occur at higher frequencies. Although the FEM developed for the X-56A includes vibration modes for the nose boom, these modes occur at frequencies higher than those excited during this maneuver.

Angle of Attack

Air flow angle vanes are often used to measure angle of attack and flank angle. The angle-of-attack output measurement for a sensor at D is

$$\alpha_D = \arctan\left(\frac{w_D}{u_D}\right)$$

$$= \arctan\left(\frac{w - q(x_s + \phi_{k_x}\eta_k) + p(y_s + \phi_{k_y}\eta_k) + \phi_{k_z}\dot{\eta}_k}{u - r(y_s + \phi_{k_y}\eta_k) + q(z_s + \phi_{k_z}\eta_k) + \phi_{k_x}\dot{\eta}_k}\right) \tag{50}$$

from substitution of equations (26a)–(26c).

This equation can be simplified by assuming that η is much smaller than $\dot{\eta}$ and therefore can be ignored. If, in addition, low angles of attack, low angular rates, and high speeds can be assumed, the output equation reduces to

$$\alpha_D = \alpha + \frac{p\,y_s - q\,x_s + \phi_{k_z}\dot{\eta}_k}{V} \tag{51}$$

which shows the most important contributions to the measurement, besides the angle of attack, are from the angular rates and the modal rates. This equation is similar to the conventional position-offset correction applied to angle of attack measurements [1,3,20] to transfer the angle of attack measurement to the aircraft mass center, but includes the modal rate. The linearized versions of equation (50) are

$$\Delta\alpha_D = \left[\frac{-w_0}{u_0^2 + w_0^2}\right]\Delta u + \left[\frac{u_0}{u_0^2 + w_0^2}\right]\Delta w + \left[\frac{u_0(y_s + \phi_{k_y}\eta_{k_0})}{u_0^2 + w_0^2}\right]\Delta p$$

$$+ \left[\frac{-u_0(x_s + \phi_{k_x}\eta_{k_0}) - w_0(z_s + \phi_{k_z}\eta_{k_0})}{u_0^2 + w_0^2}\right]\Delta q$$

$$+ \left[\frac{w_0(y_s + \phi_{k_y}\eta_{k_0})}{u_0^2 + w_0^2}\right]\Delta r + \left[\frac{u_0\,\phi_{k_z} - w_0\,\phi_{k_x}}{u_0^2 + w_0^2}\right]\Delta\dot{\eta}_k \tag{52}$$

using the body axes, or

$$\Delta\alpha_D = \Delta\alpha + \left[\frac{\cos\alpha_0(y_s + \phi_{k_y}\eta_{k_0})}{V_0\cos\beta_0}\right]\Delta p$$

$$+ \left[\frac{-\cos\alpha_0(x_s + \phi_{k_x}\eta_{k_0}) - \sin\alpha_0(z_s + \phi_{k_x}\eta_{k_0})}{V_0\cos\beta_0}\right]\Delta q$$

$$+ \left[\frac{\sin\alpha_0(y_s + \phi_{k_y}\eta_{k_0})}{V_0\cos\beta_0}\right]\Delta r + \left[\frac{\phi_{k_z}\cos\alpha_0 - \phi_{k_x}\sin\alpha_0}{V_0\cos\beta_0}\right]\Delta\dot{\eta}_k \tag{53}$$

using the stability axes. These linearization are similar to those for rigid aircraft but include the modal rate contribution.

Flight test data in figures 3–4 show that the short period and SW1B modes affected the measured data, whereas the SW1T mode did not. This is because angle of attack strongly participates in the classical short period mode, and because ϕ_{7_z} was large along the air data boom, as shown in figure 5. The SW1T mode, however, did not have a large mode shape ϕ_{9_z} at the sensor position.

Flank Angle and Sideslip Angle

Similar to the angle of attack, an air flow angle vane is often used to measure flank angle. The output measurement equation for a sensor at D is

$$\mu_D = \arctan\left(\frac{v_D}{u_D}\right)$$

$$= \arctan\left(\frac{v + r(x_s + \phi_{k_x}\eta_k) - p(z_s + \phi_{k_z}\eta_k) + \phi_{k_y}\dot{\eta}_k}{u - r(y_s + \phi_{k_y}\eta_k) + q(z_s + \phi_{k_z}\eta_k) + \phi_{k_x}\dot{\eta}_k}\right) \tag{54}$$

The output can again be reduced by assuming negligible vibration mode displacements, low aerodynamic flow angles, low angular rates, and high speeds, so that the flank angle is approximately

$$\mu_D = \mu + \frac{rx_s - pz_s + \phi_{k_y}\dot{\eta}_k}{V} \tag{55}$$

Again, these assumptions are questionable for subscale aircraft [20]. The flank angle is related to the sideslip angle and angle of attack as

$$\beta = \arctan(\tan\mu\cos\alpha) \tag{56}$$

Using this relation and under these assumptions, $\mu \simeq \beta$ and equation (55) becomes

$$\mu_D = \beta + \frac{rx_s - pz_s + \phi_{k_y}\dot{\eta}_k}{V} \tag{57}$$

Again, this is the conventional position-offset correction applied to flank angle measurements [1, 3, 20] with an additional modal rate term.

Linearizing the flank angle output with the body axes produces

$$\begin{aligned}\Delta\mu_D = &\left[\frac{-v_0}{u_0^2+v_0^2}\right]\Delta u + \left[\frac{u_0}{u_0^2+v_0^2}\right]\Delta v + \left[\frac{-u_0(z_s+\phi_{k_z}\eta_{k_0})}{u_0^2+v_0^2}\right]\Delta p \\ &+ \left[\frac{-v_0(z_s+\phi_{k_z}\eta_{k_0})}{u_0^2+v_0^2}\right]\Delta q + \left[\frac{u_0(x_s+\phi_{k_x}\eta_{k_0}) + v_0(y_s+\phi_{k_y}\eta_{k_0})}{u_0^2+v_0^2}\right]\Delta r \\ &+ \left[\frac{u_0\,\phi_{k_y} - v_0\,\phi_{k_x}}{u_0^2+v_0^2}\right]\Delta\dot{\eta}_k\end{aligned} \tag{58}$$

or, using the stability axes,

$$\begin{aligned}\Delta\mu_D = &\left[V_0^2\cos\alpha_0\right]\frac{\Delta\beta}{\Gamma_0} + \left[V_0^2\sin\alpha_0\sin\beta_0\cos\beta_0\right]\frac{\Delta\alpha}{\Gamma_0} \\ &+ \left[-V_0\cos\alpha_0\cos\beta_0(z_s+\phi_{k_z}\eta_{k_0}\right]\frac{\Delta p}{\Gamma_0} + \left[-V_0\sin\beta_0(z_s+\phi_{k_z}\eta_{k_0}\right]\frac{\Delta q}{\Gamma_0} \\ &+ \left[V_0\cos\alpha_0\cos\beta_0(x_s+\phi_{k_x}\eta_{k_0}) + V_0\sin\beta_0(y_s+\phi_{k_y}\eta_{k_0})\right]\frac{\Delta r}{\Gamma_0} \\ &+ \left[\phi_{k_y}V_0\cos\alpha_0\cos\beta_0 - \phi_{k_x}V_0\sin\beta_0\right]\frac{\Delta\dot{\eta}_k}{\Gamma_0}\end{aligned} \tag{59}$$

where the common denominator

$$\Gamma_0 = V_0^2(\cos^2\alpha_0\cos^2\beta_0 + \sin^2\beta_0) \tag{60}$$

was factored for convenience.

5 Conclusions

In this report, output measurement equations for sensors commonly used in flight dynamics analyses were developed. These equations incorporated the effects of a deforming aircraft structure, which was represented using an expansion of orthogonal mode shapes. The output equations included linear and angular accelerometers, strain gauges, rate gyroscopes, Euler angles, airspeed, and air-flow angle measurements. Afterwards, various assumptions were explored and applied to simplify the output equations. Flight data from the X-56A aeroelastic demonstrator were discussed for context.

The output measurement equations developed in this report may be generalized in several ways. First, more realistic sensor models can be obtained by including other effects such as measurement noise, bias errors, time delays, etc. These effects were omitted in this report to focus on the structural deformation contributions. Second, more general parameterizations of the aircraft structural deformation could be used to model nonlinear deformations, such as with larger HALE-type aircraft. Linear superpositions of orthogonal vibration mode shapes were used in this report because this parameterization is typically useful and insightful, and because aeroelastic analyses are traditionally performed using linear models.

Assumptions were explored to simplify the output equations for a variety of conditions. In some cases, nonlinearities were simplified and/or some of the contributions of the structural deformation were neglected. In other cases, the output equations were linearized to provide first-order approximations that could be assembled into transfer function or state-space models typically used in flight dynamics-related work such as simulation, feedback control design, and system identification.

In determining which output equations to use for a specific purpose, it is recommended to first consider the flexibility of the aircraft, bandwidth of the relevant structural resonances, and goals for the analysis. From there, the full output equations should be simplified as much as possible. The equations compiled and discussed in this report can, in many cases, provide those equations, or if not, they can provide guidance for obtaining those equations.

6 Acknowledgements

This research was supported by the NASA Advanced Air Transport Technology (AATT) project. The efforts of the X-56A team at NASA Armstrong Flight Research Center are gratefully acknowledged. Eugene Morelli, Carlos Roithmayr, John Ryan, and David Schmidt performed technical reviews that improved the quality of this report. Several insightful discussions with David Schmidt are acknowledged and appreciated.

References

1. Gainer, T.; and Hoffman, S.: "Summary of Transformation Equations and Equations of Motion Used in Free-Flight and Wind-Tunnel Data Reduction and Analysis". SP-3070, NASA, Hampton, VA, 1972.

2. Gracey, W.: "Measurement of Aircraft Speed and Altitude". RP-1046, NASA, Hampton, VA, May 1980.

3. Morelli, E.; and Klein, V.: *Aircraft System Identification: Theory and Practice,* 2nd edition. Sunflyte Enterprises, Williamsburg, VA, 2016.

4. McRuer, D.; Ashkenas, I.; and Graham, D.: *Aircraft Dynamics and Automatic Control*. Princeton University Press, 1973.

5. Maine, R.: "Aerodynamic Derivatives for an Oblique Wing Aircraft Estimated from Flight Data by Using a Maximum Likelihood Technique". TP-1336, NASA, Edwards, CA, October 1978.

6. Schmidt, D.: *Modern Flight Dynamics*. McGraw-Hill, 2012.

7. Schwanz, R.; and Wells, W.: "Estimation of Elastic Aircraft Parameters using the Maximum Likelihood Method". *Parameter Estimation Techniques and Applications in Aircraft Flight Testing*, H. Rediess, ed., no. TN D-7647, NASA, Edwards, CA, April 1974, pp. 337–358.

8. Theodore, C.; Ivler, C.; Tischler, M.; Field, E.; Neville, R.; and Ross, H.: "System Identification of a Large Flexible Transport Aircraft". No. 2008-6894 in AIAA Atmospheric Flight Mechanics Conference, Honolulu, HI, August 2008.

9. de Oliveira Silva, B.; and Mönnich, W.: "System Identification of Flexible Aircraft in Time Domain". No. 2012-4412 in AIAA Atmospheric Flight Mechanics Conference, Minneapolis, MN, August 2012.

10. Beranek, J.; Nicolai, L.; Burnett, E.; Atkinson, C.; Holm-Hansen, B.; and Flick, P.: "Conceptual Design of a Multi-utility Aeroelastic Demonstrator". No. 2010-9350 in 13th AIAA/ISSMO Multidisciplinary Analysis Optimization Conference, Forth Worth, TX, September 2010.

11. Ryan, J.; Bosworth, J.; Burken, J.; and Suh, P.: "Current and Future Research in Active Control of Lightweight, Flexible Structures Using the X-56 Aircraft". No. 2014-0597 in AIAA SciTech, National Harbor, MD, January 2014.

12. Kane, T.; and Levinson, D.: *Dynamics: Theory and Applications*. McGraw-Hill, 1985.

13. Shearer, C.; and Cesnik, C.: "Nonlinear Flight Dynamics of Very Flexible Aircraft". *Journal of Aircraft*, vol. 44, no. 5, September–October 2007, pp. 1528–1545.

14. Chang, C.-S.; Hodges, D.; and Patil, M.: "Flight Dynamics of Highly Flexible Aircraft". *Journal of Aircraft*, vol. 45, no. 1, March–April 2008, pp. 538–545.

15. Haering, E.: "Airdata Calibration Techniques for Measuring Atmospheric Wind Profiles". *Journal of Aircraft*, vol. 29, no. 4, July-August 1992, pp. 632–639.

16. Maine, R.; and Iliff, K.: "Application of Parameter Estimation to Aircraft Stability and Control: The Output-Error Approach". RP-1168, NASA, Edwards, CA, June 1986.

17. Duke, E.; Antoniewicz, R.; and Krambeer, K.: "Derivation and Definition of a Linear Aircraft Model". RP-1207, NASA, Edwards, CA, August 1988.

18. Chan, H.; Parker, A.; Piazza, A.; and Richards, W.: "Fiber-optic sensing system: Overview, development and deployment in flight at NASA". 2015 IEEE Avionics and Vehicle Fiber-Optics and Photonics Conference, Nov 2015, pp. 71–73.

19. Grauer, J.; and Boucher, M.: "Real-Time Parameter Estimation for Flexible Aircraft". No. 2018-3155 in Atmospheric Flight Mechanics Conference, AIAA, Atlanta, GA, 2018.

20. Grauer, J.: "Position Corrections for Airspeed and Flow Angle Measurements on Fixed-Wing Aircraft". TM-2017-219795, NASA, Hampton, VA, November 2017.

Appendix A — Derivation of Accelerometer Outputs

The accelerometer output can be derived using Newton's second law applied to a rigid aircraft with constant mass at the mass center $B^\star$

$$\sum \mathbf{f} = \frac{{}^N d}{dt}(m\,{}^N\mathbf{v}^{B^\star})$$

$$= m\left(\frac{{}^B d}{dt}({}^N\mathbf{v}^{B^\star}) + \boldsymbol{\omega}\times{}^N\mathbf{v}^{B^\star}\right) \tag{A-1}$$

where $\mathbf{f}$ are applied forces on the aircraft. Considering only forces due to aerodynamics, propulsion, and gravity, this equation expands to

$$\mathbf{f}_a + \mathbf{f}_p + \mathbf{f}_g = m\left(\frac{{}^B d}{dt}({}^N\mathbf{v}^{B^\star}) + \boldsymbol{\omega}\times{}^N\mathbf{v}^{B^\star}\right) \tag{A-2}$$

where

$$\mathbf{f}_a = \bar{q}SC_X\,\mathbf{b}_1 + \bar{q}SC_Y\,\mathbf{b}_2 + \bar{q}SC_Z\,\mathbf{b}_3 \tag{A-3}$$

$$\mathbf{f}_p = X_p\,\mathbf{b}_1 + Y_p\,\mathbf{b}_2 + Z_p\,\mathbf{b}_3 \tag{A-4}$$

$$\mathbf{f}_g = (-mg\sin\theta)\,\mathbf{b}_1 + (mg\sin\phi\cos\theta)\,\mathbf{b}_2 + (mg\cos\phi\cos\theta)\,\mathbf{b}_3 \tag{A-5}$$

Equation (A-2) can be rearranged as

$$\frac{1}{m}(\mathbf{f}_a + \mathbf{f}_p) = \frac{{}^B d}{dt}({}^N\mathbf{v}^{B^\star}) + \boldsymbol{\omega}\times{}^N\mathbf{v}^{B^\star} - \frac{1}{m}\mathbf{f}_g \tag{A-6}$$

which is discussed in more detail below.

Linear accelerometers measure the specific forces acting on the aircraft, excluding the gravitational force [3, 16]. In steady level flight, 1 g of downward acceleration due to gravity is balanced by 1 g of upward acceleration due to lift. However, a vertical accelerometer will register 1 g of upward acceleration because the gravitational contribution is excluded from the output. According to this description, the equation for an accelerometer output at the mass center $B^\star$ of a rigid aircraft is equal to the left side of equation (A-6)

$$g\,\boldsymbol{a}^{B^\star} = \frac{1}{m}(\mathbf{f}_a + \mathbf{f}_p) \tag{A-7a}$$

or, equivalently, the the right side of equation (A-6)

$$g\,\boldsymbol{a}^{B^\star} = \frac{{}^B d}{dt}({}^N\mathbf{v}^{B^\star}) + \boldsymbol{\omega}\times{}^N\mathbf{v}^{B^\star} - \frac{1}{m}\mathbf{f}_g \tag{A-7b}$$

Note that $\boldsymbol{a}$ is used for the accelerometer output, whereas $\mathbf{a}$ is used for the kinematic acceleration. Although accelerometer measurements are typically provided in g units, the factor g remains on the left side of the equations in this report for convenience.

The first form of the accelerometer output, given in equation (A-7a), is written in terms of the applied forces on the aircraft, excluding gravity. It may be the simpler of the two forms, and is often used in aircraft parameter estimation when the applied forces are of primary interest [3, 16], and also in simulation applications because the applied forces are computed to solve the equations of motion. The second form of the accelerometer output, given in equation (A-7b), uses the aircraft states and their derivatives, and is potentially more complex than the first form. This form is commonly used in flight dynamics analyses and transfer function models because of its explicit dependence on the aircraft states [4, 6, 8].

When accelerometers are not located at the aircraft mass center, additional accelerations are registered by the sensor. Using equation (5), the corrections

$$g\,\boldsymbol{a}^{D} = g\,\boldsymbol{a}^{B^{\star}} + 2\boldsymbol{\omega}\times{}^{B}\mathbf{v}^{D} + \boldsymbol{\alpha}\times(\mathbf{r}^{B^{\star}C} + \mathbf{r}^{CD}) + \boldsymbol{\omega}\times[\boldsymbol{\omega}\times(\mathbf{r}^{B^{\star}C} + \mathbf{r}^{CD})] + {}^{B}\mathbf{a}^{D} \tag{A-8}$$

are applied to equation (A-7a) or (A-7b) to account for these additional terms. Scalar expansions of the output are presented as equations (28a)–(28c) and (34a)–(34c) for the first and second forms, respectively. When the local structural deformation, velocity, and acceleration are all zero, the conventional accelerometer position offset corrections [1] are recovered.

Figures

Figure 1: X-56A airplane (credit: NASA / Jim Ross).

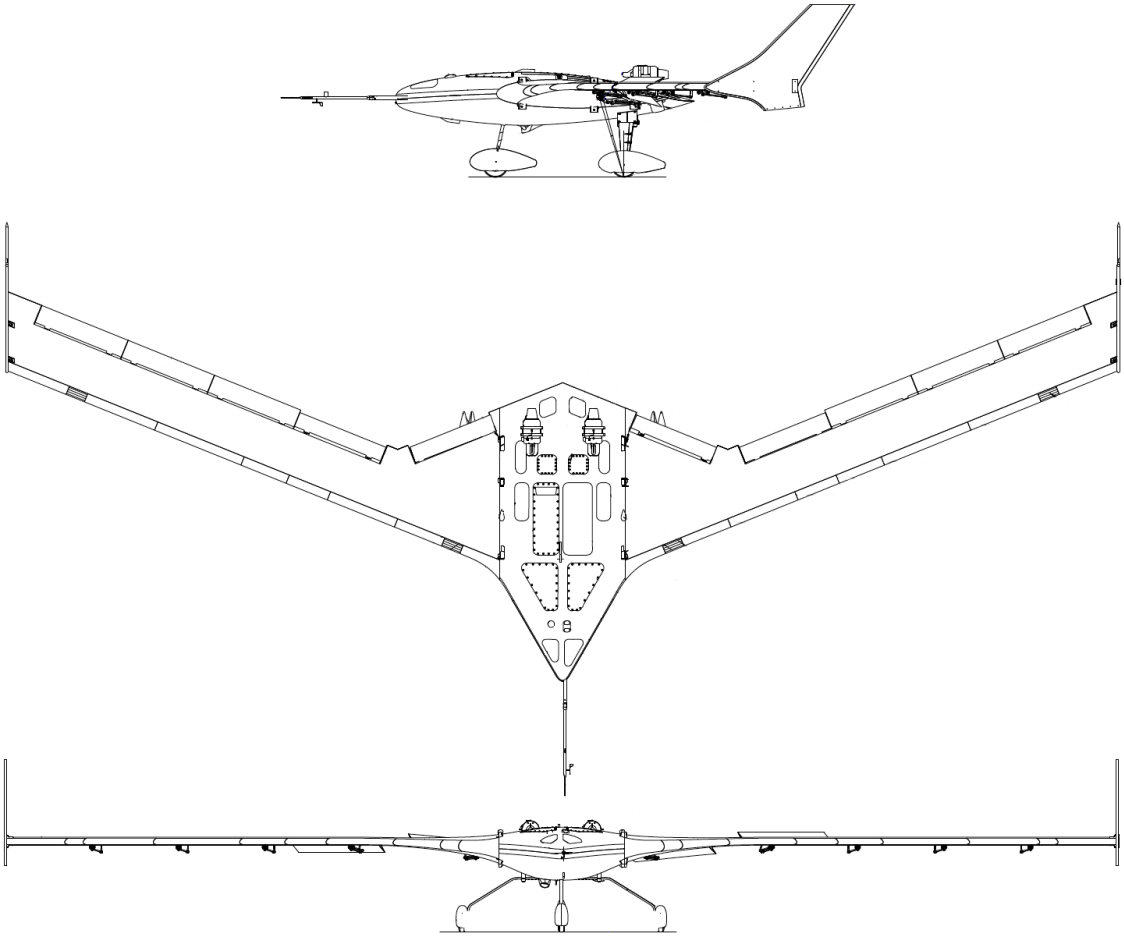

Figure 2: Three-view drawing of the X-56A.

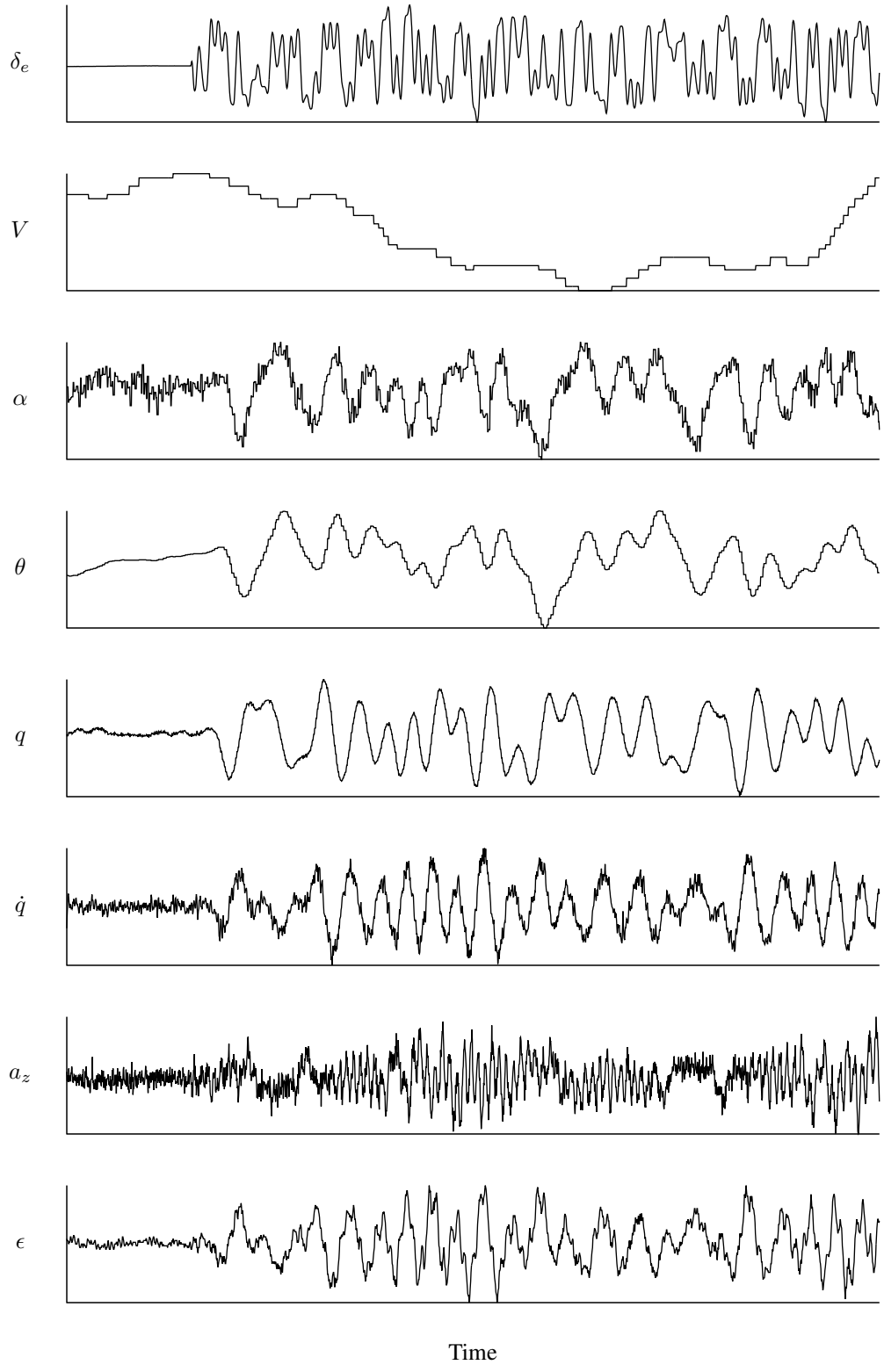

Figure 3: Measured flight test data for the X-56A (Phase 1, Flight 11, FTA 300).

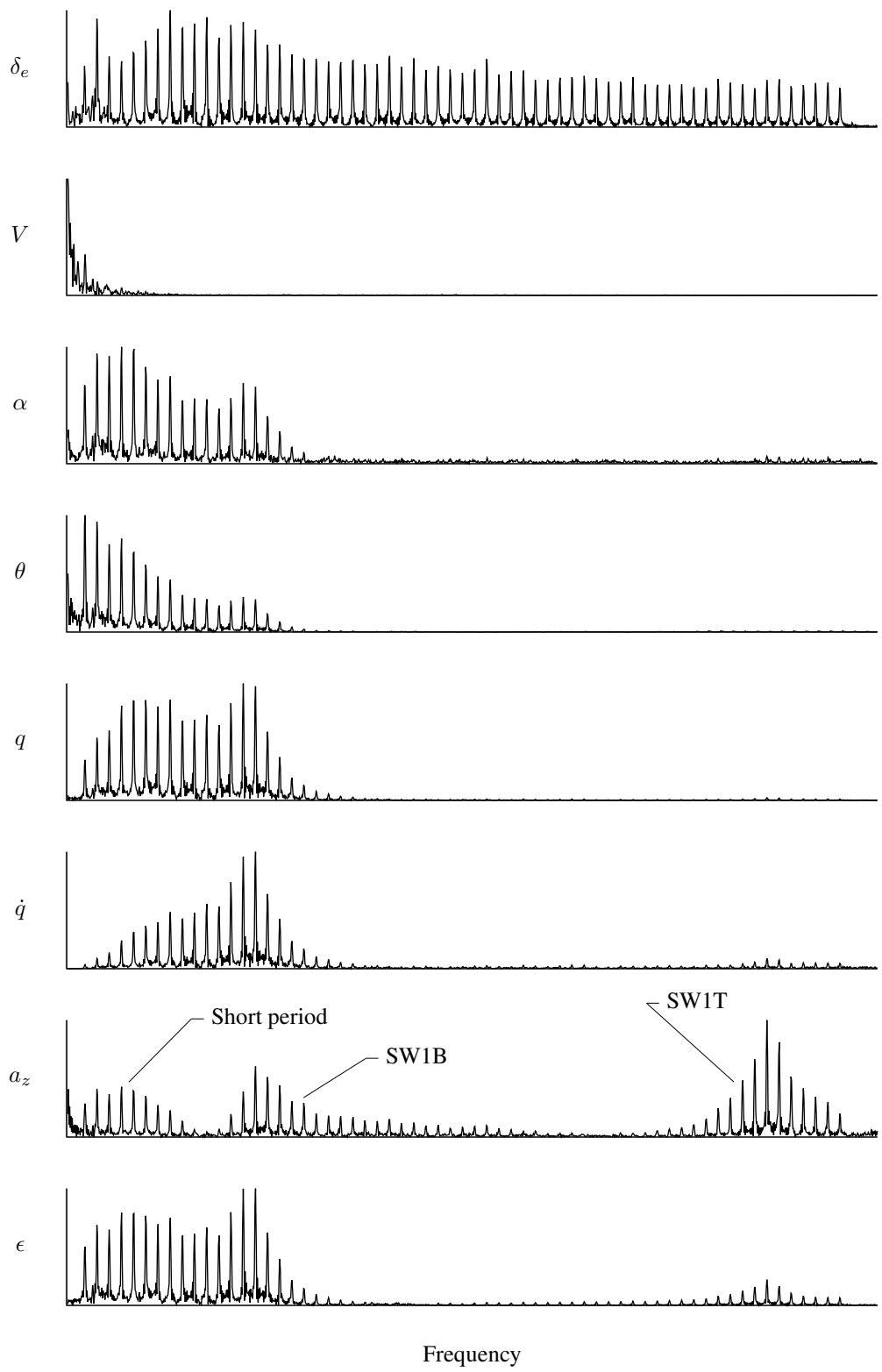

Figure 4: Amplitude spectra of the X-56A measurements.

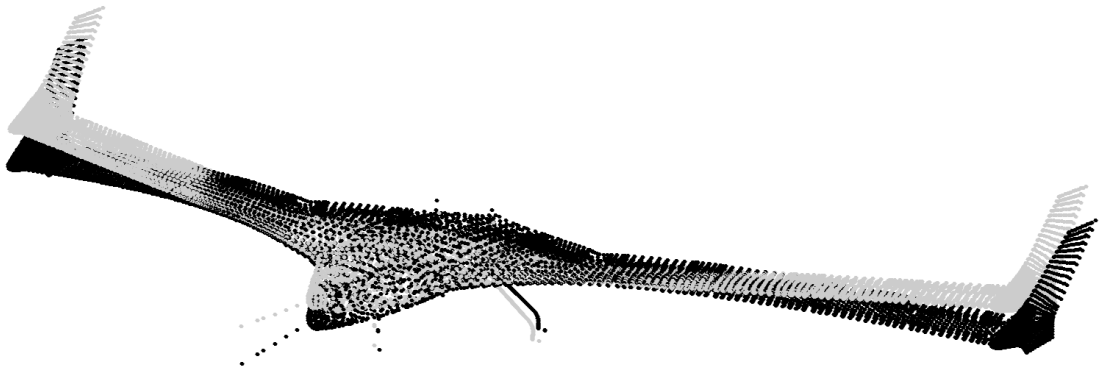

(a) Mode 7: first symmetric wing bending (SW1B).

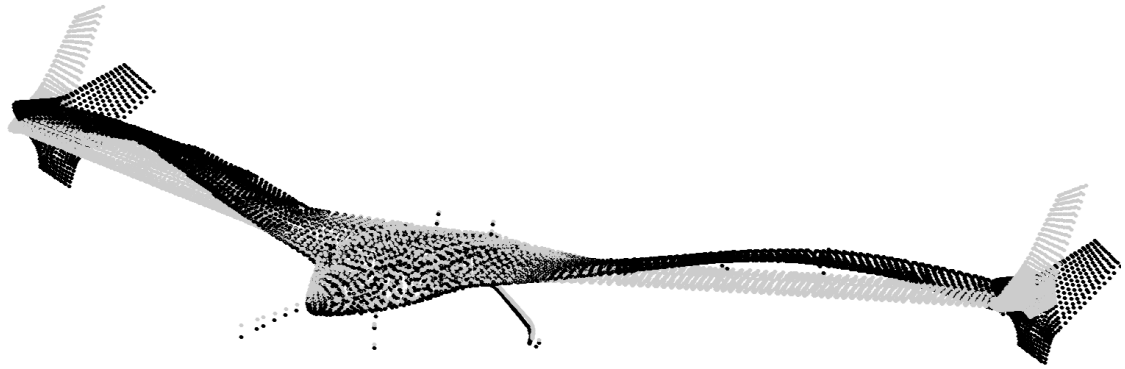

(b) Mode 9: first symmetric wing torsion (SW1T).

Figure 5: Scaled mode shapes for the X-56A (FEM configuration 24611, version 10.424, 50% fuel); gray dots are the undeformed grid points and black dots are the corresponding deformed points.

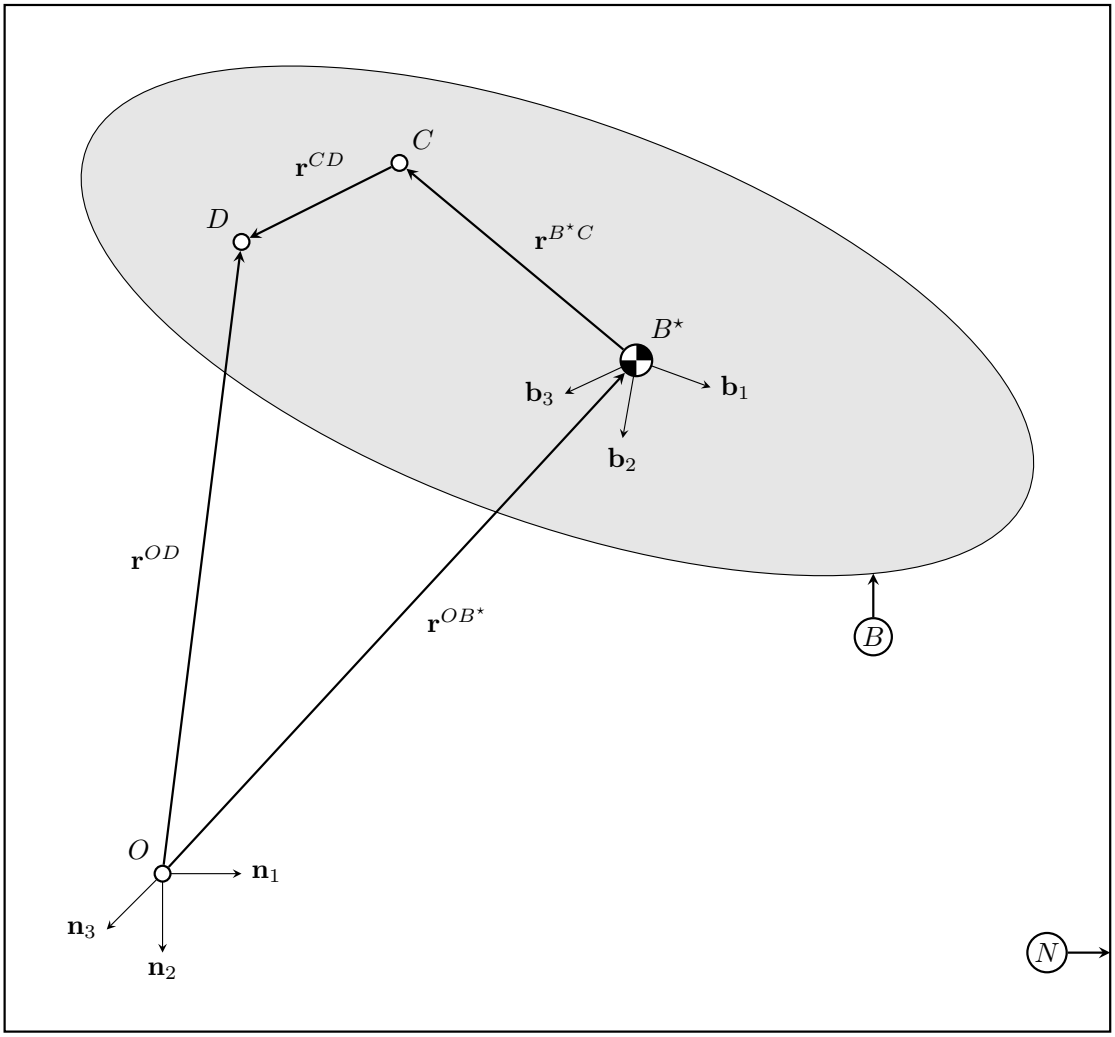

Figure 6: Schematic for a generic flexible aircraft.

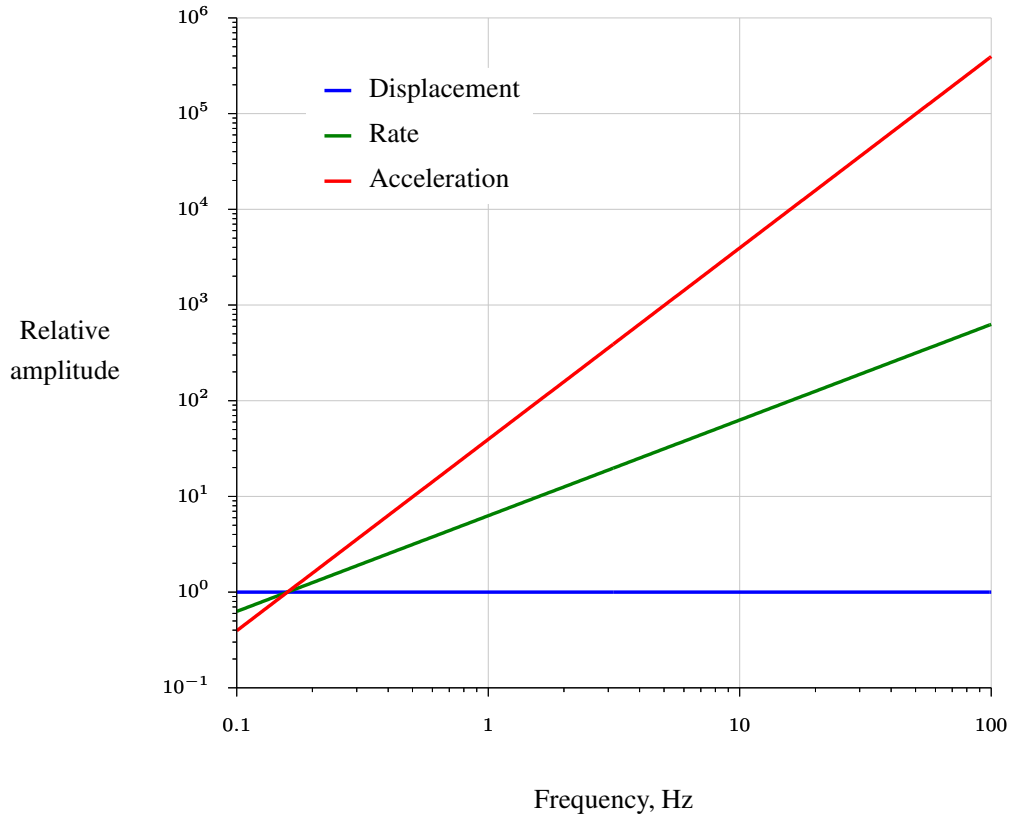

Figure 7: Variation of vibration mode displacement, rate, and acceleration relative amplitudes with frequency.

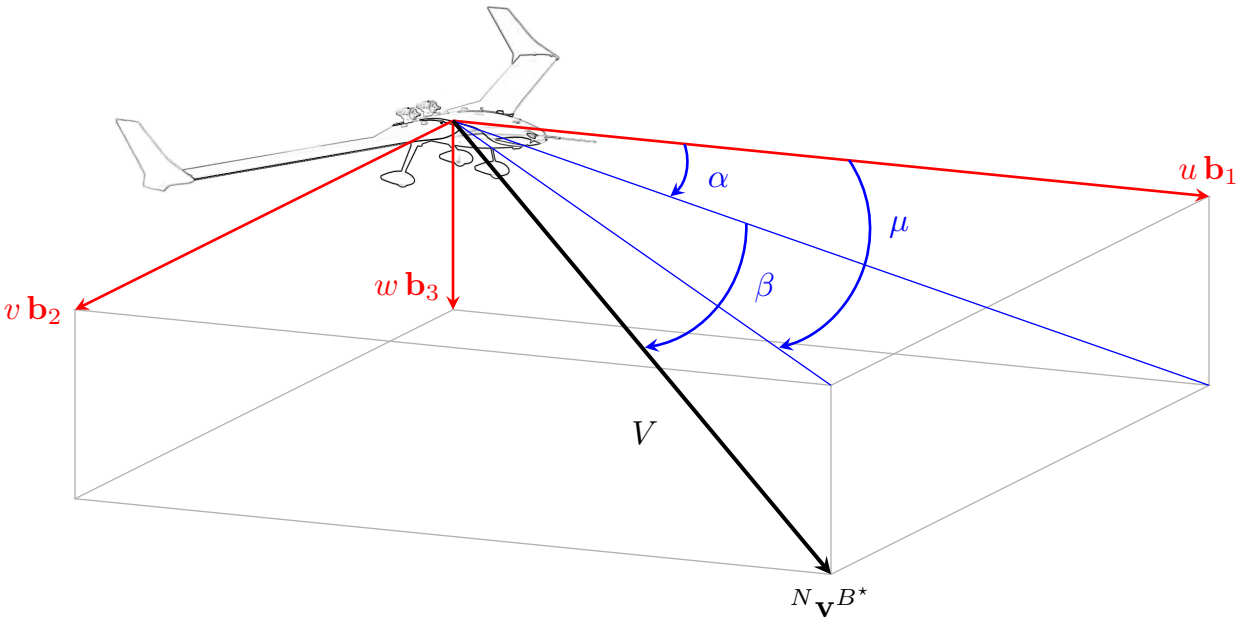

Figure 8: Velocity component and aerodynamic flow angle definitions.

REPORT DOCUMENTATION PAGE	Form Approved OMB No. 0704–0188

1. REPORT DATE *(DD-MM-YYYY)*	2. REPORT TYPE	3. DATES COVERED *(From - To)*
01-10-2018	Technical Memorandum	

4. TITLE AND SUBTITLE

Output Measurement Equations for Flexible Aircraft Flight Dynamics

5a. CONTRACT NUMBER

5b. GRANT NUMBER

5c. PROGRAM ELEMENT NUMBER

6. AUTHOR(S)

Jared A. Grauer
Langley Research Center, Hampton, Virginia

Matthew J. Boucher
Armstrong Flight Research Center, Edwards, California

5d. PROJECT NUMBER

5e. TASK NUMBER

5f. WORK UNIT NUMBER
081876.02.07.02.01.01

7. PERFORMING ORGANIZATION NAME(S) AND ADDRESS(ES)
NASA Langley Research Center
Hampton, Virginia 23681-2199

8. PERFORMING ORGANIZATION REPORT NUMBER
L–20956

9. SPONSORING/MONITORING AGENCY NAME(S) AND ADDRESS(ES)
National Aeronautics and Space Administration
Washington, DC 20546-0001

10. SPONSOR/MONITOR'S ACRONYM(S)
NASA

11. SPONSOR/MONITOR'S REPORT NUMBER(S)
NASA/TM–2018–220102

12. DISTRIBUTION/AVAILABILITY STATEMENT
Unclassified-Unlimited
Subject Category 08
Availability: NASA STI Program (757) 864-9658

13. SUPPLEMENTARY NOTES

14. ABSTRACT

A summary of output measurement equations for onboard sensors used in flight testing flexible aircraft is presented. These equations include the effects of structural flexibility and are considerably more complex than the standard equations for rigid-body aircraft. The output equations discussed include accelerations from linear and angular accelerometers, strains, angular rates, Euler angles, true airspeed, and air flow angles. The output equations are derived in full form and then simplified. Linearized output equations, suitable for state-space or transfer function models, are also developed. Example flight test data from the X-56A subscale aeroelastic demonstrator is discussed for reference.

15. SUBJECT TERMS
Measurement equations, Flexible aircraft, Aeroelasticity, Flight Dynamics

16. SECURITY CLASSIFICATION OF:			17. LIMITATION OF ABSTRACT	18. NUMBER OF PAGES	19a. NAME OF RESPONSIBLE PERSON
a. REPORT	b. ABSTRACT	c. THIS PAGE			STI Help Desk (email: help@sti.nasa.gov)
U	U	U	UU	36	19b. TELEPHONE NUMBER *(Include area code)* (757) 864-9658